

GAS PHASE REACTION KINETICS OF BORON FIBER PRODUCTION

**A THESIS SUBMITTED TO
THE GRADUATE SCHOOL OF NATURAL AND APPLIED SCIENCES
OF
THE MIDDLE EAST TECHNICAL UNIVERSITY**

BY

FATİH FIRAT

**IN PARTIAL FULFILLMENT OF THE REQUIREMENTS FOR THE
DEGREE OF
MASTER OF SCIENCE
IN
THE DEPARTMENT OF CHEMICAL ENGINEERING**

JUNE 2004

Approval of the Graduate School of Natural and Applied Sciences.

Prof. Dr. Canan ÖZGEN
Director

I certify that this thesis satisfies all the requirements as a thesis for the degree of Master of Science.

Prof. Dr. Timur Dođu
Head of Department

This is to certify that we have read this thesis and that in our opinion it is fully adequate, in scope and quality, as a thesis for the degree of Master of Science.

Assoc. Prof. Dr. N. Aslı Sezgi
Co-Supervisor

Prof. Dr. H. Önder Özbelge
Supervisor

Examining Committee Members

Prof. Dr. Hayrettin Yücel

Prof. Dr. H. Önder Özbelge

Prof. Dr. Suna Balcı

Assoc. Prof. Dr. Naime Aslı Sezgi

Assist. Prof. Dr. Halil Kalıpçılar

ABSTRACT

GAS PHASE REACTION KINETICS OF BORON FIBER PRODUCTION

Firat, Fatih

M.S., Department of Chemical Engineering

Supervisor: Prof. Dr. H. Önder Özbelge

Co-supervisor: Assoc. Prof. Dr. Naime Aslı Sezgi

June 2004, 92 pages

In the production of boron fibers using CVD technique, boron deposition and dichloroborane formation reactions take place in a reactor. Boron deposition reaction occurs at the surface while formation of dichloroborane is the result of both gas phase and surface reactions.

A CSTR type of reactor was designed and constructed from stainless steel to investigate the gas phase reaction kinetics and kinetic parameters of boron fibers produced from the reaction of boron trichloride and hydrogen gases in a CVD reactor. The gases were heated by passing through the two pipes which were located into the ceramic furnace and they were mixed in the CSTR. The effluent gas mixture of the reactor was quenched by passing through a heat exchanger. An FT-IR spectrophotometer was connected to the heat exchanger outlet stream to perform on-

line chemical analysis of the effluent gas mixture. Experiments were carried out at atmospheric pressure and a reactor temperature range of 300-600 °C with different inlet reactant concentrations. The analysis of the FT-IR spectra indicated that the gas phase reaction and the surface reaction started at reactor temperatures above 170 °C and 500°C, respectively. It was concluded that reaction rate of the product increased with an increase in the inlet concentration of both reactants (BCl_3 and H_2) and with an increase in the reactor temperature. The gas phase reaction rate was expressed in terms of a^{th} and b^{th} orders with respect to the inlet concentrations of BCl_3 and H_2 . The activation energy of the gas phase reaction, a and b were found to be 30.156 kJ/mol , 0.54 and 0.64, respectively. The correlation coefficient was 0.9969.

Keywords: CVD, Boron Fiber Production, Gas Phase Reaction Kinetics, Dicloroborane.

ÖZ

BOR FİBER ÜRETİMİ GAZ FAZ REAKSİYON KİNETİĞİ

Fırat, Fatih

Yüksek Lisans, Kimya Mühendisliği Bölümü

Tez Yöneticisi: Prof. Dr. H. Önder Özbelge

Yardımcı Yönetici: Doç. Dr. Naime Aslı Sezgi

Haziran 2004, 92 sayfa

Kimyasal buhar biriktirme tekniği kullanılarak bor elyafı üretiminde, reaktörde bor birikim ve $BHCl_2$ oluşum reaksiyonları gerçekleşmektedir. Bor birikim reaksiyonu yüzeyde gerçekleşirken, $BHCl_2$ oluşum reaksiyonu hem yüzeyde hem de gaz fazında gerçekleşmektedir.

Kimyasal buhar biriktirme reaktöründe H_2 ve BCl_3 gazlarının reaksiyonu sonucunda üretilen bor fiberlerinin gaz faz reaksiyon kinetiğinin ve kinetik parametrelerinin araştırılması için CSTR tipi bir reaktör tasarlanıp, paslanmaz çelikten yapılmıştır. Gazlar reaktöre girmeden önce seramik fırın içerisine yerleştirilen iki borudan geçerek ısıtılmaktadır ve daha sonra CSTR'da karışmaktadır. Reaktörden çıkan gaz karışımı ısı değiştiriciden geçerek soğutulmaktadır. FT-IR spektrofotometresi ısı değiştiricinin çıkışına bağlanarak

ıkan gazın kimyasal analizi yapılmaktadır. Deneyler atmosferik basınta, 300-600°C arasında deęiřen reaktör sıcaklık aralıęında, gazların farklı giriř konsantrasyonlarında gerekleřmektedir. FTIR spektrumları gaz faz reaksiyonunun ve yüzeş reaksiyonlarının sırasıyla 170°C ve 500°C'nin üzerindeki reaktör sıcaklıklarında gerekleřtięini göstermiřtir. Ürünlerin reaksiyon hızının, BCl₃ ve H₂'nin giriř konsantrasyonları ve reaktör sıcaklıęındaki artıřlarla artıř gösterdięi sonucuna varılmıřtır. Gaz faz reaksiyon hızı BCl₃ ve H₂'nin a. ve b. dereceden üstleri řeklinde ifade edilmiřtir. Gaz faz reaksiyonun aktivasyon enerjisi, a ve b sırasıyla 0.54, 0.64 ve 30.156 *kJ/mol* olarak bulunmuřtur. Korelasyon sabiti 0.9969' dur.

Anahtar Kelimeler: Kimyasal Buhar Biriktirme, Bor Elyafı Üretimi, Gaz Faz Reaksiyon Kinetięi, Dikloroboran

*To my parents,
who always support me in all aspects of my life*

ACKNOWLEDGEMENTS

I express my sincere appreciation to Prof. Dr. H. Önder Özbelge and Assoc. Prof. Dr. Naime Aslı Sezgi for their guidance, supports and valuable contributions throughout this study. I gratefully acknowledge Mr. Mustafa Karaman for his help in the preparation of the experimental setup and the performance of calibration experiments.

I would like to thank the technicians of Chemical Engineering Department for their help in the manufacturing of double pipe heat exchanger and reactor used in the experimental setup.

Finally, I express my deepest gratitude to my mother, Siddıka Fırat and my father, Halil Fırat for their encouragements throughout my education life.

TABLE OF CONTENTS

ABSTRACT	iii
ÖZ	v
ACKNOWLEDGEMENTS	viii
TABLE OF CONTENTS	ix
LIST OF TABLES	xi
LIST OF FIGURES	xiv
LIST OF SYMBOLS	xvi
CHAPTERS	
1. INTRODUCTION	1
1.1. Boron Fiber Production Methods.....	9
1.1.1. Thermal Decomposition Process.....	9
1.1.2. Chemical Vapor Deposition Method	11
1.2. Literature Survey.....	14
1.3. Objectives of the Present Work.....	20
2. EXPERIMENTAL PART	22
2.1. Experimental Set-up.....	23
2.2. Experimental Procedure.....	28
3. RESULTS AND DISCUSSION	35
3.1 Chemical Analysis of Reactant Outlet Stream.....	35

3.2 Reaction Rate of Each Species and the Conversion of Gas Phase Reaction	38
3.3 Reproducibility of the Experimental Data	42
3.4 Data Acquisition Method	42
3.5 Results for BCl ₃ -H ₂ Experiments.....	45
3.6 Results for BCl ₃ -H ₂ -He Experiments.....	52
3.7 Evaluation of Rate Parameters of the Proposed Rate Expression.....	57
4. CONCLUSION	60
REFERENCE	
CALIBRATION METHODS	66
A.1 Calibration Method for BCl ₃ Concentration Measurement	66
A.2 Calibration Method for Hydrochloric Acid Concentration Measurement ..	71
CALCULATIONS FOR DOUBLE PIPE HEAT EXCHANGER.....	73
B.1. Temperature Profile along the Length of the Heat Exchanger.....	80
EXPERIMENTAL DATA	82
THE RESIDENCE TIME DISTRIBUTION OF REACTOR	87

LIST OF TABLES

1.1. Chemical Properties of Boron.....	4
1.2. Atomic Structure of Boron.....	5
1.3. Physical Properties of Boron.....	6
1.4. Comparison of Tensile Properties of Boron with Other Materials	8
2.1. Experimental Conditions for BCl ₃ -H ₂ Experiments (Tot. Vol. Flowrate: 209.07 ml/min, y _{BCl₃} =0.025 and y _{H₂} =0.975).....	31
2.2. Experimental Conditions for BCl ₃ -H ₂ Experiments (Tot. Vol. Flowrate: 211.02 ml/min, y _{BCl₃} =0.034 and y _{H₂} =0.966).....	31
2.3. Experimental Conditions for BCl ₃ -H ₂ Experiments (Tot. Vol. Flowrate: 213.62 ml/min, y _{BCl₃} =0.046 and y _{H₂} =0.954).....	31
2.4. Experimental Conditions for BCl ₃ -H ₂ Experiments (Tot. Vol. Flowrate: 215.7 ml/min, y _{BCl₃} =0.058 and y _{H₂} =0.942).....	32
2.5. Experimental Conditions for BCl ₃ -H ₂ -He Experiments (Tot. Vol. Flowrate: 207.18 ml/min, y _{BCl₃} =0.066, y _{H₂} =0.086 and y _{He} =0.848).....	32
2.6. Experimental Conditions for BCl ₃ -H ₂ -He Experiments (Tot. Vol. Flowrate: 207.25ml/min, y _{BCl₃} =0.066, y _{H₂} =0.115 and y _{He} =0.819).....	32
2.7. Experimental Conditions for BCl ₃ -H ₂ -He Experiments (Tot. Vol. Flowrate: 207.31ml/min, y _{BCl₃} =0.066, y _{H₂} =0.143 and y _{He} =0.791).....	33

2.8. Experimental Conditions for BCl ₃ -H ₂ -He Experiments (Tot. Vol. Flowrate: 207.38 ml/min, y _{BCl₃o} =0.066, y _{H₂o} =0.172 and y _{He} =0.762).....	33
2.9. Experimental Conditions for BCl ₃ -H ₂ -He Experiments (Tot. Vol. Flowrate: 207.44 ml/min, y _{BCl₃o} =0.066, y _{H₂o} =0.200 and y _{He} =0.734).....	33
2.10. Experimental Conditions for BCl ₃ -H ₂ -He Experiments (Tot. Vol. Flowrate: 207.52 ml/min, y _{BCl₃o} =0.066, y _{H₂o} =0.228 and y _{He} =0.706).....	34
2.11. Experimental Conditions for Reproducibility of Experiment BCl ₃ -4 (Tot. Vol. Flowrate: 218.2 ml/min, y _{BCl₃o} =0.065 and y _{H₂o} =0.935).....	34
B.1. Temperature Change of Helium with Length of Heat Exchanger.....	81
C.1. The Raw Data for BCl ₃ -H ₂ Experiments (Tot. Vol. Flowrate: 209.07 ml/min, y _{BCl₃o} =0.025 and y _{H₂o} =0.975).....	83
C.2. The Raw Data for BCl ₃ -H ₂ Experiments (Tot. Vol. Flowrate: 211.02 ml/min, y _{BCl₃o} =0.034 and y _{H₂o} =0.966).....	83
C.3. The Raw Data for BCl ₃ -H ₂ Experiments (Tot. Vol. Flowrate: 213.62 ml/min, y _{BCl₃o} =0.046 and y _{H₂o} =0.954).....	83
C.4. The Raw Data for BCl ₃ -H ₂ Experiments (Tot. Vol. Flowrate: 215.7 ml/min, y _{BCl₃o} =0.058 and y _{H₂o} =0.942).....	84
C.5. The Raw Data for BCl ₃ -H ₂ -He Experiments (Tot. Vol. Flowrate: 207.18 ml/min, y _{BCl₃o} =0.066, y _{H₂o} =0.086 and y _{He} =0.848)	84
C.6. The Raw Data for BCl ₃ -H ₂ -He Experiments (Tot. Vol. Flowrate: 207.25ml/min, y _{BCl₃o} =0.066, y _{H₂o} =0.115 and y _{He} =0.819)	84
C.7. The Raw Data for BCl ₃ -H ₂ -He Experiments (Tot. Vol. Flowrate: 207.31ml/min, y _{BCl₃o} =0.066, y _{H₂o} =0.143 and y _{He} =0.791)	85

C.8. The Raw Data for $\text{BCl}_3\text{-H}_2\text{-He}$ Experiments (Tot. Vol. Flowrate: 207.38 ml/min, $y_{\text{BCl}_3}=0.066$, $y_{\text{H}_2}=0.172$ and $y_{\text{He}}=0.762$)	85
C.9. The Raw Data for $\text{BCl}_3\text{-H}_2\text{-He}$ Experiments (Tot. Vol. Flowrate: 207.44 ml/min, $y_{\text{BCl}_3}=0.066$, $y_{\text{H}_2}=0.200$ and $y_{\text{He}}=0.734$)	85
C.10. The Raw Data for $\text{BCl}_3\text{-H}_2\text{-He}$ Experiments (Tot. Vol. Flowrate: 207.5 ml/min, $y_{\text{BCl}_3}=0.066$, $y_{\text{H}_2}=0.228$ and $y_{\text{He}}=0.706$)	86
C.11. The Raw Data of Reproducibility (Tot. Vol. Flowrate: 218.2 ml/min, $y_{\text{BCl}_3}=0.065$ and $y_{\text{H}_2}=0.935$).....	86
D.1 Residence Time Distribution Experiment for Determination of the Steady State Time of Gas Cell	89
D.2 The Raw Data for the Residence Time Distribution Experiment	90

LIST OF FIGURES

1.1 A Schematic Diagram of CVD Reactor	12
2.1. Schematic Diagram of Reactor and Furnace.....	25
2.2. Heat Exchanger	26
2.3. Schematic Diagram of Experimental Set-up.....	27
3.1 FTIR Spectrum of Gas Mixture before Heating the Reactor	36
3.2 FTIR Spectrum of Gas Mixture after Heating the Reactor	37
3.3 Change of HCl Mole Fraction in the Reactor Effluent Stream as a Function of Temperature	43
3.4 Change of BCl ₃ Mole Fraction in the Reactor Effluent Stream as a Function of Temperature	43
3.5 Steady State Outlet Mole Fractions of BCl ₃ , HCl and BHCl ₂ (Total Volumetric Flow Rate: 207.18 ml/min, T _r =490°C, y _{BCl₃0} =0.066, y _{H₂} =0.086, y _{He} =0.848)	44
3.6 Effect of Initial Mole Fraction of BCl ₃ on Conversion for Different Reactor Temperatures.....	46
3.7 Effect of Temperature on Conversion for Different Inlet Compositions of BCl ₃	47
3.8 Effect of Temperature on Mole Fraction of BHCl ₂ for Different Inlet Compositions of BCl ₃	48
3.9 Effect of Temperature on the Ratio of BHCl ₂ Mole Fraction to the HCl Mole Fraction	50

3.10 Effect of Temperature on Reaction Rate of HCl for Different Inlet Compositions of BCl ₃	51
3.11 Change of Conversion with Different Inlet Compositions of H ₂ at Various Reactor Temperatures	53
3.12 Effect of Inlet Mole Fraction of H ₂ on Conversion for Different Reactor Temperatures.....	54
3.13 Effect of Temperature on the Mole Fraction of BHCl ₂ for Different Inlet Compositions of H ₂	55
3.14 Change of Reaction Rate of HCl as a Function of Reactor Temperature for Different Inlet Compositions of H ₂	56
3.15 Graph for the Predicted and the Experimental Reaction Rate of HCl	58
3.16 Predicted Reaction Rate of HCl versus Residual Values of Model Equation.....	59
A.1. Calibration Set-up for Boron Trichloride.....	68
A.2. Calibration Curve for Boron Trichloride at a Wavenumber Range of 1100-850 cm ⁻¹	70
A.3. Calibration Curve for Hydrochloric Acid at a Wavenumber of 2798 cm ⁻¹	72
B.1. The Temperature Profile of Helium in the Heat Exchanger.....	81
D.1. Experimental Set-up for Characterization of Reactor	88
D.2 Change of Methane Peak Height with Time for the Gas Cell.....	91
D.3 Change of Methane Peak Height with Time for Reactor and Gas Cell	91
D.4 Change of Methane Peak Height with Time for Reactor Only, Obtained by Taking the Difference of Curves Given in Figure D.2 and Figure D.3	92

LIST OF SYMBOLS

a	Surface area per volume of packing,	m^2/m^3
a	th. order with respect to boron trichloride,	
A'	Heat transfer area,	m^2
A	Cross sectional area,	m^2
$Area$	Peak area,	
b	th. order with respect to hydrogen,	
C	Capacity rate ratio,	
C	Concentration,	$kmol/m^3$
C_p	Specific heat,	$kJ/kg \cdot K$
D_p	Nominal diameter of ceramic saddle rings,	m
D'	Diameter of outer pipe,	m
D	Diameter of inner pipe,	m
f_p	Bed fouling factor,	$1/m$
F	Molar flow rate,	$kmol/s$
F_T	Total molar flow rate of gas mixture,	$kmol/s$
G	Mass velocity,	$kg/m^2 \cdot s$
E_a	Activation Energy,	$kJ/kmol \cdot K$

h	Heat transfer coefficient,	$watt/m^2 \cdot K$
H	Height,	m
L	Length of the heat exchanger,	m
k	Thermal conductivity,	$watt/m \cdot K$
k_o	Frequency factor,	$\frac{(m^3)^{0.18}}{s \cdot (kmol)^{0.18}}$
m	Mass flow rate,	kg/s
M	Molecular weight,	$kg/kmol$
Nre	Reynolds Number,	
Npr	Prandtl Number,	
NTU	Number of transfer unit,	
Δx	Thickness of inner pipe,	m
Q	Heat transfer rate of heat exchanger,	$watt$
Q	Inlet mole fraction ratio of reactants,	
P	Pressure,	atm
R	Ideal gas constant,	$atm \cdot m^3/kmol \cdot K$
R	Reaction rate,	$kmol/m^3 \cdot min$
t	Total time necessary to reach steady state,	min
T_e	Temperature of the heat exchanger effluent stream,	$^{\circ}C$
T_f	Temperature of furnace,	$^{\circ}C$
T_r	Temperature of reactor,	$^{\circ}C$
T_s	Set point temperature of the controller,	$^{\circ}C$
T_{in}	The inlet temperature,	K
T_a	The average temperature,	K

T_{out}	Outlet temperature,	K
T_w	Wall temperature of the heat exchanger interface,	K
U	Overall heat transfer coefficient,	$watt/m^2 \cdot K$
W	Weight,	kg
v	Linear velocity,	m/s
\dot{V}	Volumetric flow rate,	m^3/s
V_R	Volume of reactor,	m^3
y	Mol fraction,	
x	Conversion,	

Greek Symbols

ε_o	Void fraction of packing,	
ε	Heat exchanger effectiveness,	
μ	Viscosity,	$kg/m \cdot s$
μ_w	Viscosity at wall temperature,	$kg/m \cdot s$
ρ	Density,	kg/m^3

Subscripts

p	Packing material
w	Wall of inner pipe
c	Cold fluid (water)
f	Final

<i>h</i>	Hot fluid (helium)
<i>i</i>	Inner tube
<i>o</i>	Outer tube
<i>o</i>	Inlet
min	Minimum
max	Maximum
<i>mix</i>	Gas mixture (H ₂ +BCl ₃)
<i>rxn</i>	Reaction

CHAPTER 1

INTRODUCTION

The engineering of modern composite materials has had a significant impact on the technology of design and construction. By combining two or more materials together, we are now able to make advanced composite materials which are lighter, stiffer and stronger than any other structural materials man has ever used (Vinson, 1975).

Composite materials are obtained from the combination of two or three solids. The physical properties of advanced composites are superior to the metallic structural materials when they are compared according to their density. Their performance is very high due to their density. Thus, they are generally used in the production of lightweight structural compounds.

The success that has been made in the development of boron composites, metal matrix composites, and, more recently, in carbon-carbon composites has showed the ever increasing potential of composite materials.

Boron, which is located in group III-A of the periodic table, is a black solid element. It is classified as a metalloid. It has some specific properties, such as

hardness and brittleness (Sezgi, 1996). Boron is used as reinforcing agent to strengthen the materials. It is added to pure metals, alloys or to other solids such as silica to make them strong against the mechanical and the thermal damages.

Boron occurs in nature and is found in the form of borates in the oceans, sedimentary rocks, coal, shale and some soils. It is nonmetallic, with an atomic number of 5 and a relative atomic mass of 10.811. It has excellent physical and chemical properties when compared with the other materials. Boron is widely distributed in nature, with concentrations of around 10 mg/kg in the land's surface and around 4.5 mg/lit in the ocean (Chiang, 1997). The most important commercial borate products and minerals are borax pentahydrate, borax, sodium perborate, boric acid, tinkal, colemanite and ulexite. Economic borate deposits are rare, and exist in Turkey, USA, Argentina, Chile, Russia, China and Peru.

Total world production of boron minerals such as colemanite, $\text{Ca}_2\text{B}_6\text{O}_{11}\cdot 5\text{H}_2\text{O}$; ulexite, $\text{CaNaB}_5\text{O}_9\cdot 8\text{H}_2\text{O}$; tincal, $\text{Na}_2\text{O}\cdot 2\text{B}_2\text{O}_3\cdot 4\text{H}_2\text{O}$; kernite, $\text{Na}_2\text{B}_4\text{O}_7\cdot 4\text{H}_2\text{O}$; probertit, $\text{NaCaB}_5\text{O}_9\cdot 5\text{H}_2\text{O}$; hidroboraksit, $\text{CaMgB}_6\text{O}_{11}\cdot 6\text{H}_2\text{O}$ was approximately 2,750,000 tones in 1994. About 800,000 tons of commercial borate products were manufactured from boron minerals. Turkey has the largest reserves of boron in the world. About 70 percent of the world boron reserves exist in Turkey. These boron reserves are located especially at the Western Anatolia in Marmara Region. Boron minerals are mined around Bandırma, Balıkesir and Kütahya. Turkish boron ores were found in Bigadiç which is a county of Balıkesir in 1900, in Mustafakemalpaşa in 1954, in Emet and Hisarcık counties in 1956 and in Seyitgazi and Kırka in 1968. Boron is processed and sold by Eti Holding. A total of 200,000 tons of boron were produced in 1998 and that Emet Etibor Corporation sold boron mineral worth of seven trillion Turkish liras in 1998 (Alınç, 2003).

First studies in the production of boron fibers have begun in 1960's. After 1985, advances which have been accomplished by CVD method, this area attracted more attention (Buck, 1987). AVCO Specialty Materials, which is located in USA, is the first firm to produce boron fiber.

The production technology of boron fiber materials has been developed with the production of composite materials. Boron thin films are used in special areas such as electronics, high temperature applications, and nuclear reactors and in sun batteries (Yalaz, 1987). One of the hardness to the usage of boron fiber is its high cost compared to that of other fibers. A major portion of this high price is the cost of the tungsten substrate.

Boron fibers have shown superior average tensile strength of 3.45×10^9 N/m² and elastic modulus of 4.14×10^{11} N/m². The density of boron fiber is 2.6 g/cm³ and is close to that of glass (Vinson, 1975).

Boron fibers are the reinforcing materials most commonly used in high performance composites. Fiber is defined as the load bearing component of composite materials. It is a general term for a filament with a finite length that is at least 100 times its diameter (typically 10^{-4} to 1.3×10^{-4} m). For a material to be a fiber, it must have high thermal stability and should not contract or expand much with temperature. Defects can be placed on the surface to allow for the fiber to interact with the substrate, however; bulk defects should be low. In most cases, fibers are prepared by drawing from a molten bath, spinning or deposition on a substrate.

The term fiber is often used synonymous with filament. Some specific criteria are necessary for a material to be called as fiber. These are high tensile modulus and tensile strength, high impact resistance, high stiffness and high dimensional stability (low coefficient of expansion) and surface reactions are necessary to produce fiber.

Continuous boron filaments have been developed which have a high degree of expectation for application in high strength and high modulus composites. The specific strength of boron fiber is comparable to those of glass fibers and is much higher than those of metallic filaments. The ratio of modulus to density is especially noteworthy because it is about five times greater than the same ratio of glass filaments which are commonly used in composite applications. Also the specific modulus of boron is higher than the metallic filaments with the exception of beryllium. The specific modulus of boron and beryllium are comparable; the specific strength of beryllium is only one-third of that of boron (Vinson, 1975). The hardness of boron is also significant since boron is much less sensitive than glass to damage during handling. That is why; hardness and tensile strength are the most important properties of boron. Mechanical properties of boron are superior when it is compared with other metals. Chemical, atomic and physical properties of boron are given in Table 1.1 to 1.3.

Table 1.1. Chemical Properties of Boron (Kirk Othmer, 1992)

Chemical Properties of Boron	
Electrochemical Equivalent	0.1344 g/amp-hr
Electron Work Function	4.45 eV
Electronegativity (Pauling)	2.04
Heat of Fusion	50.2 kJ/mol
Ionization Potential	
First	8.298
Second	25.154
Third	37.93
Valance Electron Potential	190 (-eV)

Table 1.2. Atomic Structure of Boron (Kirk Othmer, 1992)

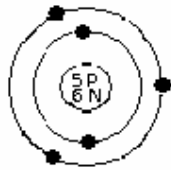
Atomic Structure of Boron	
Atomic Radius	1.17 Å
Atomic Volume	4.6 cm ³ /mol
Covalent Radius	0.82 Å
Cross Section	759 barns
Crystal Structure	Tetragonal, α and β -rhombohedral
Electron Configuration	1s ² 2s ² p ¹
Electrons per Energy Level	2.3
Shell Model	
Ionic Radius	0.23 Å
Filling Orbital	2p ¹
Number of Electrons	5 (with no charge)
Number of Neutrons	6 (most common)
Number of Protons	5
Oxidation States	3
Valance Electrons	2s ² p ¹

Table 1.3. Physical Properties of Boron (Kirk Othmer, 1992)

Physical Properties of Boron	
Atomic Mass Average	10.811
Boiling Point	4275K, 4002°C, 7236°F
Coefficient of Linear Thermal Expansion	0.0000083 cm/cm/°C (0°C)
Electrical Conductivity	1.0E -12 /cm
Thermal Conductivity	0.274 W/cm.K
Density	2.34 g/cm ³ at 300K
Description	Black, non-metallic crystal
Enthalpy of Atomization	573.2 kJ/mole at 25°C
Enthalpy of Fusion	22.18 kJ/mole
Enthalpy of Vaporization	480 kJ/mole
Specific Heat	1.02 J/g.K
Hardness Scale	
Mohs	9.3
Vickers	49000 MN m ⁻²
Tensile Strength	3.45x10 ⁹ N/m ²
Elastic Modulus	4.14x10 ¹¹ N/m ²
Heat of Vaporization	489.7 kJ/mol
Melting Point	2573K 2300°C 4172°F
Molar Volume	4.68 cm ³ /mole
Physical State (at 20°C & 1atm)	Solid
Vapor Pressure	0.348 Pa at 2300°C
Index of Refraction	5790 Å by using Hg lamp

Boron deposition temperatures which are available in the literature for the various forms of boron are not always consistent. The structure of the deposited material appears to be highly dependent on the reactant gas used and its purity. This is the reason for this consistency. Amorphous boron can be obtained at high temperatures from BCl_3 by keeping the contact time of the reactant gases extremely short. Conversely, at temperatures which give amorphous boron, crystalline boron of the β -rhombohedral configuration has been obtained by adding a small percentage of HCl to the reactant gases or by returning decomposition products of the reaction to the heated zone (Park, 2001).

The boron fiber surface shows a "corn-cob" structure consisting of nodules separated by boundaries. The nodule size varies during the course of preparation. In a very general way, the nodules start as individual nuclei on the substrate and then grow outward in a conical form until a filament diameter of 80-90 micron is reached, above which the nodules seem to decrease in size (Mahan, 2000).

One of the prominent attributes of boron filaments is their extremely high modulus. A measure of the true potential of a material for aerospace applications can be realized from values called the specific strength and specific modulus (this is the strength or modulus divided by the density of the material). These values of boron filaments are absolutely perfect and exclusive. Table 1.4 shows a comparison of the filaments with other potential materials. These data show boron filaments to be incomparable in the combination of specific strength and specific modulus (Lawrence, 1967).

Surface reactions are far more difficult to probe under realistic process conditions and are difficult to predict theoretically. However, techniques for measuring the rates of gas phase reactions are well developed, highly reactive,

intermediate species that may play an important role in CVD are often difficult to detect and study. On the other hand, the gas phase kinetic calculation was investigated more and it is well known. Fortunately, theoretical approaches to predicting the thermochemistry and kinetics of gas phase processes are well established, at least for main group species in the first and second rows of the periodic table (Allendorf, 1998).

Table 1. 4. Comparison of Tensile Properties of Boron with Other Materials.

Materials	Strength		Modulus	
	Average psi x 10 ³	Strength in. x 10 ⁶	Average psi x 10 ³	Strength in. x 10 ⁶
Continuous boron filament	400	4.0	60	600
E-glass filament	500	5.4	10.5	110
Beryllium	90	1.3	44	660
Steel	28 to 600	0.1 to 2.1	30	110
Titanium	60 to 240	0.1 to 1.5	19	120
Aluminum	9.8 to 88	0.1 to 0.9	9.8	100
Magnesium	25 to 55	0.4 to 0.9	6	100

Gas phase reactions can be divided into two basic types: bond dissociation reactions, which proceed without an activation barrier, and more complex reactions, such as atom abstractions, molecular eliminations, or isomerizations, in which an energy barrier exists (Allendorf, 1998).

Simulating the gas phase chemistry in a CVD reactor requires more than chemistry. Rate constants for the reactions that occur are also necessary to understand the time evolution of the gas phase and correctly identify the species interact with the surface. As in the case of thermochemistry, experimental

investigations have not kept pace with the demand for such data. In some cases, theoretical approaches can be used to identify structures of reaction transition states and to determine Arrhenius parameters, although their accuracy is not as high as when predicting heats of formation (Allendorf, 1998).

In the literature and in the industry, gas phase reactions are tried to be minimized by impinging the reactants toward the substrate. Since 1960's, scientists have been studying to find out the surface reaction mechanism of boron fiber produced in impinging jet reactors. The first boron fiber was fabricated in 1959 by Talley. Since then, the technology of boron fiber fabrication has developed with the investigations. The most common production methods of boron fiber are given below.

1.1. Boron Fiber Production Methods

The production methods of boron fibers are developing with the development of technology. There are several methods for boron fiber production in the literature. But there are commercially two methods available for the production of boron fibers. These are chemical vapor deposition and thermal decomposition methods. The remaining methods are not as efficient and usable as these two methods. The detailed information about these methods is given in the following items.

1.1.1. Thermal Decomposition Process

All substances are unstable above certain temperatures. The main theory for the deposition rates of substances is that reactant gas molecules begin to break down

and produce small cluster on the substrate surface which are called nuclei or active sites. After the reaction proceeds, the number of nuclei and their size increase. In spite of the several researches done about the thermal decomposition process, the kinetic pattern of this process has still not been understood. Thermal decomposition method is widely used in industry, such as rotary kiln in the cement industry. In this process deposition process is performed at reduced pressures.

By using thermal decomposition process, it is also possible to produce boron fibers. In this method, a substrate is heated up to a temperature necessary to perform the decomposition process in a chamber which initially contains diborane. Decomposition reaction takes place on the substrate surface. Diborane is decomposed on the substrate surface. Boron fibers are produced on the substrate surface according to the following reaction;



More than two species are generated in the decomposition process. In the reaction given above, boron fibers and H₂ are obtained. In the reaction, the diborane is directly taken into the reaction chamber or pressurized by using pressure atomizer. Before taken into the pressure atomizer, diborane is dissolved in an appropriate solvent and admitted into the deposition chamber. The droplets with a size of 1 to 1000 μm are produced. These small droplets are directly impinged toward the heated substrate. The impingement of these droplets supplies uniformity and fastness to the process. This process is carried out at a temperature range of 450 to 650°C with a pressure range of 0.3 to 3 kPa. The structure of the produced by using this method is amorphous (Yalaz, 1987).

1.1.2. Chemical Vapor Deposition Method

Chemical vapor deposition is widely used in thin film technology. CVD is defined as a method in which gaseous reactants are diffused toward a heated solid material called substrate and deposited on to the substrate surface. The major application of this method is the coating of surfaces, but also it is used for the production of high purity materials.

Boron fiber production is one of the thin film applications of CVD method. In this process, very high temperatures are required and, a refractory material is needed, for example, a high melting point metal such as tungsten, as a substrate. It turns out that such metals are also very dense. The density of tungsten is 19.254 g/cm^3 (Kirk-Othmer, 1992). The boron fibers produced by this method have a very high and uniform quality. The boron is deposited by chemical vapor deposition of a mixture of boron trihalide (BX_3), especially boron trichloride (BCl_3) and hydrogen (H_2) on a solid material which heated up to a high temperature range of 1000-1400°C.



The boron is deposited in the form of small clusters onto the surface filament. Some of the boron atoms actually penetrate the filament and cause the filament to expand in diameter. A typical diameter for a boron coated tungsten fiber changes in a range of 100-140 μm (Ersoy, 1997). Boron coated aluminum fibers are used in the space shuttle industry. However, their wide usage area has been restricted due to their high cost. Figure 1.2 shows a typical arrangement of CVD reactor for the production of boron fibers.

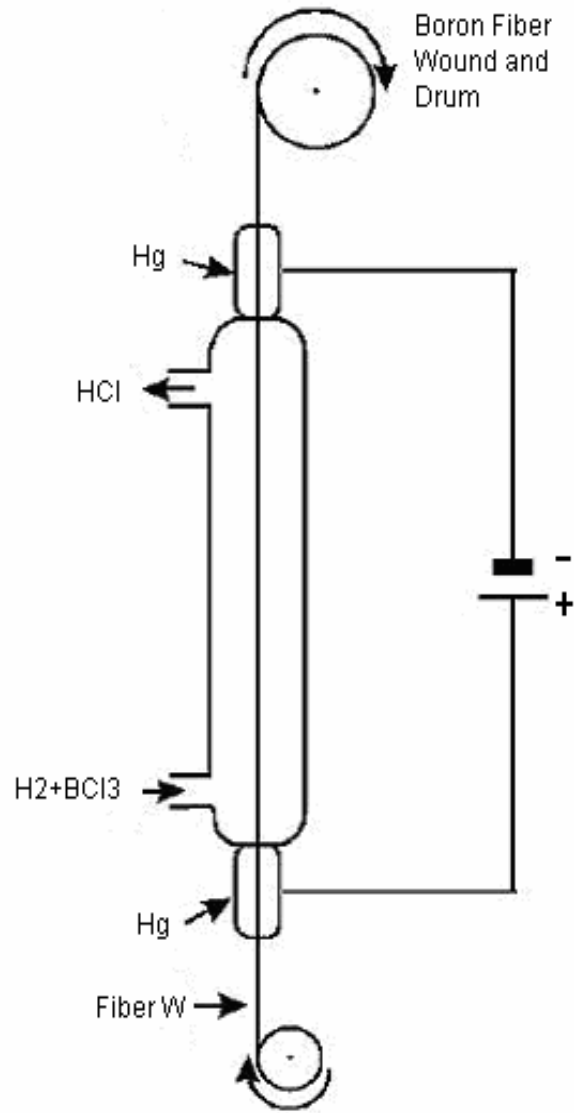


Figure 1.1 A Schematic Diagram of CVD Reactor

The substrate wire, which is pulled through the chamber by substrate feed, is heated electrically to the desired temperature. There are mercury containers at the inlet and outlet of the substrate wire. Mercury serves as electrical contacts as well as gas seal in the chambers. The substrate is cleaned by an outlet gas or cleaning chamber before entering the deposition chamber. A mixture of the desired reactant gas is passed through the deposition chamber at positive pressure where it contacts the heated wire and deposits boron.

In this process, there is a critical temperature to obtain a boron fiber with optimum properties and structure. There are three crystallographic structures of boron. These are amorphous, α and β -rhombohedral. The desirable β -rhombohedral form of boron occurs below this critical temperature. The β -rhombohedral boron has approximately crystalline size of $1\mu\text{m}$. β -rhombohedral is thermodynamically stable form of boron and known to have superior mechanical properties over the other forms. It is a very important strategy to obtain this structure in continuous boron fiber production. With the substrate wire stationary in the reactor, this critical temperature is about 1300°C (Ersoy, 1997). In a system where the wire is moving, this critical temperature is higher and it increases with the speed of the wire. Higher wire drawing speed also results in an increase in production rate and lower costs.

In general, CVD is classified in various ways depending on the conditions of the reaction chamber such as low and high pressure, plasma assisted, cold and hot wall, close and open system. Most commonly, plasma assisted, the hot and cold wall reactors are commercially used. If the pressure of the reaction chamber is below 1 atm, it is called low pressure CVD (LPCVD) reactor. In the same manner, if the system operates continuously and steadily, in other words there is no accumulation, it is called open system. All these CVD methods are open systems.

In hot wall reactor, chamber is heated up to a high temperature, thus the substrate placed in the chamber to be coated and the other parts included by this chamber are also heated to the same temperature of chamber. On the other hand, in cold wall reactor, only the substrate placed into the chamber is heated. Cold wall reactor is more complex and requires more control than hot wall reactor, because there is a natural convection phenomenon in cold wall reactor. The surrounding temperature is not the same with the temperature of substrate. This causes the flow

pattern of the gas to be more complicated. Also, a temperature profile occurs around the substrate depending on the reactor geometry. In plasma assisted reactor, the chemical reactions in the vapor phase are activated by the creation of the plasma in the gas phase, or by directing a laser beam into the gas mixture (Park, 2001).

The main problem in the CVD kinetic studies is the complexity of the deposition process. The difficulty arises not only from the steps of the CVD process, but also from the temperature and concentration gradient; geometric effects, and the gas flow patterns in the reaction chamber. There are several possible rate limiting factors. The most predominant ones are mass transfer and surface kinetics. Mass transfer control exists, if the transfer of the reactants and reaction products across the boundary layer determines the deposition rate. If the mass transfer through the boundary layer is sufficiently large, the system is controlled by surface kinetic reactions.

1.2. Literature Survey

The deposition of boron from BCl_3 and H_2 vapors is a complex process which has been studied in details, but which is still a matter of conflict for scientists. The reaction is heterogeneous and the deposition rate likely to be limited by the surface reactions or diffusion, generally diffusion factors were studied in the case of flow perpendicular to a horizontal or vertical one (Vandelbulke, 1977).

Talley et al. (1963) showed that concentration of BCl_3 in the $\text{BCl}_3\text{-H}_2$ system was not too critical for the production of continuous boron filaments. Filaments produced from a mole percent BCl_3 range of 10-60 % have the same growth rate and strength. Deposition temperature appeared to be the most critical parameter. It was

seen that at low temperatures ($<1000^{\circ}\text{C}$) the rate on which boron is deposited is too low to be practical, whereas at high temperatures (from 1250°C to 1350°C), large crystallites often grow in certain areas along the filament.

Strength values for boron filaments are as high as any reported for a bulk material. Special testing methods had to be developed for the material. Clark et al. (1963) have developed techniques for testing boron filaments and have made a study of the mechanical properties. They showed that the tensile strength of boron filaments depends on the gage length, which is true for most materials.

Gruber (1970) investigated the chemical kinetics and the mass transport characteristics of CVD of boron by using boron trichloride and hydrogen gas mixture. In this study, it is desired to decrease the mass transfer effects as much as possible. For this reason, a reactor which provided for a stream of reactants flowing at high velocity normal to a horizontal wire was designed. In the experimental setup, a tungsten wire, which was heated up to 1200°C , was used as substrate. The tungsten wire was held between two tungsten electrodes which centered the wire in a rectangular nozzle. The tungsten electrodes were immersed into a container which was filled with mercury. As a result of the study, methods of quickly estimating rate of mass transport were indicated and Langmuir type of kinetics models for the surface reactions were suggested.

Carlton et al. (1970) worked on the rate of boron deposition by hydrogen reduction of boron trichloride at temperatures from 800 to 1400°C . In the experimental setup, the reactant gas mixture flowed at high velocity normal to a horizontal tungsten wire to decrease the mass transfer effects. The deposition rate was obtained by measuring the weight change of tungsten wire with time. Thermodynamic and kinetic analyses of the system were studied. The production of

intermediate product, dichloroborane (BHCl_2), was investigated; but it was not considered in the surface reaction kinetics. From the thermodynamic analysis, it was concluded that large amount of dichloroborane appeared to be in equilibrium with boron trichloride, hydrogen, and hydrogen chloride at the deposition surface. Also, apparent, activation energy was obtained. From the chemical analysis, Langmuir type of reaction rate mechanism was suggested. It was concluded that the rate limiting chemical step in the hydrogen reduction of boron trichloride was the reduction in the adsorbed state of dichloroborane.

Vandenbulcke and Vuillard (1977) investigated the deposition mechanisms of boron from boron trichloride and hydrogen vapors by using stagnation flow technique. They confirmed that the mechanism proposed by Carlton (1970), well describes the deposition system in various experimental conditions, especially when the vapor phase is supersaturated. Three deposition mechanisms were deduced. These are mass transfer-interfacial equilibrium, mass transfer-surface kinetics and the surface kinetics. These deposition mechanisms were studied by stagnation flow method. In this method, the reactive gas mixture streamed through a cylindrical nozzle and flowed perpendicular onto a cylindrical substrate disk to decrease the mass transfer and the gas phase effects in the reaction system. As a result, a correlation for mass transfer in impinging jets was obtained.

Krawitz and Bhardwaj (1983) studied the structure of boron in boron fibers by using boron trichloride and hydrogen as a reactant mixture. The reaction was performed in a temperature range of 1000-1400°C. Computer modeling was used to investigate the structure of noncrystalline and chemically deposited fibers. For this purpose, X-Ray diffraction patterns were obtained. The diffraction patterns from the models were computed using Debye scattering equation. The results showed that the

fibers consist of a continuous network of randomly oriented boron atoms and boron atoms arranged in icosahedra.

Michaelidis and Pollard (1984) studied the kinetic analysis of chemical vapor deposition of boron. A one dimensional model was developed which describes the interaction among hydrodynamics, multicomponent heat and mass transfer, and reaction kinetics for CVD of boron. BCl_3 and H_2 gas mixture was used to perform the reaction in an impinging jet reactor. It was concluded that BHCl_2 formation on the surface could control the deposition rate and homogeneous production of BHCl_2 had a significant effect on the process.

Pollard and Jenkinson (1984) focused on the mathematical model of CVD reactors. Thermal diffusion effects on CVD reactors were investigated. Finally, a mathematical model, which describes the behavior of CVD reactors, was derived. It was concluded that the influence of thermal diffusion on the deposition rate was dependent on the deposition system and on the operating conditions of the reactor.

Jansson (1988) et al. investigated the influence of BCl_3 , H_2 and HCl on the deposition rate of boron. In this study, a cold wall reactor was used. The influence of BCl_3 quality on the deposition rate was determined by using three different BCl_3 gases which had different purities. Moreover, the morphology of film layer produced on the substrate was examined by using scanning electron microscopy (SEM). For this purpose, thin molybdenum, α -rhombohedral boron and titanium substrate were used. It was found that the kinetics in boron CVD can be affected by the substrate material used in the deposition process. As a result, the following boron reduction rate expression was derived;

$$r = A p(\text{BCl}_3) p^n(\text{H}_2) - B p(\text{HCl})$$

With $n=0$ and $n=0.5$ for low and high partial pressures of BCl_3 , respectively. It was concluded that impurities in the BCl_3 gas affected the deposition.

Sekine et al. (1989) investigated the kinetics of boron thin film on tungsten substrate by using chemical vapor deposition method. During the experiment, rate data on the chemical vapor deposition of boron by reduction of boron trichloride with hydrogen were obtained. The reaction mechanism was determined by using these data. Activation energy of the reaction was determined. It was found that the reaction was controlled by mass transport at higher temperatures. Langmuir type reaction rate expression was suggested for the boron deposition.

Hauptfear and Schmidt (1994) studied the kinetics of boron deposition from BBr_3 and H_2 mixture by monitoring the generation of gas phase product HBr . A tantalum foil was used as the deposition substrate. The substrate was heated up to 1500°C . The outlet gas mixture was passed through the differentially pumped mass spectrometer to determine the partial pressures of the reactants and products. Film morphology, produced on the substrate, was investigated by SEM. Langmuir type reaction rate expression was proposed.

Imaishi et al. (1997) studied the macro and micro modeling of CVD synthesis. A reaction scheme in which a source of material undergoes a gas phase reaction to produce an intermediate was proposed. For this purpose, a series of simple Monte Carlo (SMC) codes was developed to simulate the observed film shape on micro trenches and holes. Surface reaction rate constants were determined using these codes. A hot wall tubular reactor was used to take the necessary data for the calculation. Gas phase reaction rate constants for single component systems were determined to simulate the experimental growth rate distributions. It was concluded that at higher temperatures, the growth rate increased with rotation speed, but at

lower temperatures the growth rate decreased with an increase in rotation speed due to is the reduced retention time in the high temperature region suppressed the gas phase reaction.

Sezgi et al. (1997) studied the dichloroborane formation during CVD of boron in a dual impinging jet reactor. The outlet gas composition was analyzed continuously by using FT-IR. In this study, the formation of dichloroborane (intermediate product) was experimentally verified. It was found that the boron deposition started at substrate temperatures around 750°C. Also, it was concluded that the fractional conversion of BCl₃ to BHCl₂ was higher than that of BCl₃ to B at low temperatures.

Sezgi et al. (1999) also investigated the mechanism of CVD of boron by hydrogen reduction of BCl₃ in a dual impinging-jet reactor. BCl₃ and H₂ gas mixture was used in the experimental set-up. The outlet gas mixture was continuously analyzed by using FT-IR. The formation of intermediate, BHCl₂ was found to take place in the gas phase and also on the surface of the substrate. The experiments were carried out at a temperature range of 750-1350°C. It was concluded that the dichloroborane formation increased with a decrease in temperature at a temperature range of 900-1350°C. The rate expressions of the surface reactions were obtained by using three different models.

Sezgi et al. (2001) studied the CVD of boron and dichloroborane formation on a hot tungsten substrate in a parallel flow reactor. Temperature effects on the formation of intermediate product BHCl₂ were investigated. The gas mixture was continuously analyzed by using FT-IR. The substrate temperature was changed between 1100-1250°C. It was concluded that BHCl₂ formation was especially formed in the gas phase rather than on the surface. Comparison of impinging and parallel

flow reactor results showed that diffusion resistance was important in parallel flow reactors. The analysis of the FT-IR spectra indicated that the formation of BHCl_2 started at a temperature of 350°C .

Dilek et al. (2001) investigated the kinetics of boron carbide formation in a dual impinging-jet reactor from a gas mixture of BCl_3 , H_2 and CH_4 . Tungsten wire was used as a substrate. The composition of reactor outlet gas mixture was determined by passing it continuously through the FT-IR. The formation of BHCl_2 was verified experimentally. The experiments were carried out at atmospheric pressure with different inlet compositions with a substrate temperature range of $1200\text{-}1450^\circ\text{C}$. It was concluded that the β -rhombohedral B_4C formation increased with an increase in the BCl_3/CH_4 ratio. But, BHCl_2 formation decreased with an increase in BCl_3 concentration in the inlet stream.

1.3. Objectives of the Present Work

As it is expressed in the literature survey that there are various type of studies accomplished about boron fibers and boron originated compounds. Boron is widely used in the advanced material technology. This is the reason for the popularity of boron among the scientists. In the literature, most of the studies are focused on the determination of surface reaction mechanism of boron on various substrates. The original objective of these studies was to obtain the necessary data to determine the deposition rate of boron on the substrate surface. Since 1960's, kinetic studies have been carried out in the production of boron fiber at different experimental conditions by using various methods and reactor types. Until the recent times, deposition rate has been determined from the weight change of substrate as a function of time. In the

last several studies, it was attempted to obtain the essential data from the chemical analysis of outlet gas mixture instead of thermogravimetric method by using special apparatus. Surface reaction mechanisms were deduced from the experimental data. But most of these studies were performed under mass transfer limitation. In the other studies, the mass transfer effects were ignored to simplify the calculations. For this purpose impinging jet reactors, which make the mass transfer effects negligible, were designed and constructed. Surface reactions occur at extremely high temperatures of substrates. In this study, the aim is to investigate the gas phase reaction of BCl_3 and H_2 . For this purpose, an experimental setup in which reactants, BCl_3 and H_2 are initially heated up to a high temperature and mixed in a CSTR was constructed to obtain the data necessary for the determination of gas phase kinetics. By using these experimental data, it is possible to develop a reaction rate expression for gas phase reaction.

In boron fiber production process, gas phase is heated up to high temperatures in the thermal boundary layer of cold wall reactors, and the bulk of the gas acquires high temperatures in the hot wall reactors. In order to achieve a comprehensive model of the CVD reactor, it is important to know the kinetics of the reaction taking place in the gas phase as well as those on the substrate surface.

CHAPTER 2

EXPERIMENTAL PART

Gas phase reactions are important for many processes in chemical industry. They bear vital importance when the temperature of the bulk gas is very high. The reason of this importance is the logarithmic increase of reaction rate constant with temperature. This relationship was derived by a chemist named Arrhenius. If the temperature increases, the reaction rate constant also increases.

In chemical vapor deposition processes, gas phase chemical reactions are important because determination of the deposition composition, film growth rates and the behavior of the reactor are dependent on the gas phase reaction. By-product formation in exhaust streams and transport of the reactants are affected by the gas phase reactions (Allendorf, 1998).

In boron fiber production, surface reactions seem to be more important than the gas phase reactions. On this account, kinetic mechanisms of surface reactions are studied by many scientists. There are various studies about the surface reaction mechanisms of boron in the literature. In the surface reactions, reactants diffuse toward the substrate and react on the surface of the substrate which is heated to a

high temperature. After the reaction, the desired product is produced on the surface. In cold wall reactors, the bulk temperature of reactants is low and not adequate for the gas phase reactions.

To be successful in this particular work, the inlet and outlet of the reactor must be well designed such that the gas phase reaction is confined to the reactor only. It must be noted that the gas phase reaction proceeds after the exit of the reactor until the bulk gas temperature decreases below a certain temperature. For these reasons, the reactants must be heated individually before they are mixed in the reactor and provision must be taken for appropriate cooling after the reactor outlet.

A continuous stirred reactor was designed and constructed with the above considerations. After the reactor, the system was completed with all the equipments, the experimental data are used to deduce the gas phase kinetics.

2.1. Experimental Set-up

A CSTR type of reactor, which was made of stainless steel with a spherical shape and volume of 0.000116 m^3 , was constructed to obtain the essential data for this study. In this reactor, two stainless steel pipes with an outside diameter of $\frac{1}{4}$ inch and 2.5 meter length were connected to the reactor. To provide the well mixing of the reactants, these pipes were fixed face to face to the reactor (Figure 2.1). Residence time distribution experiments were performed to assess how well the behavior of our reactor simulates that of a perfect CSTR, the results of these experiments are given in Appendix D. The results indicate that the change in reactor effluents for a pulse disturbance in the reactor inlet is observed within a very short time. This implies that our reactor simulates the behaviors of a perfect CSTR quite well. BCl_3 gas is fed into

the one of these pipes. H₂ and He gas mixture is given into the other pipe. The reactor with these pipes was placed near the end of a ceramic furnace in order to facilitate the easy quenching of the reactor effluent. The temperature of the furnace was measured by using a Cr-Ni thermocouple which was connected to a PID controller. The set point temperature of the controller was adjusted to the value of the desired reactor temperature. The temperature at the center of the reactor was measured by Cr-Ni thermocouple. This thermocouple was connected to a digital temperature reader. The outlet gas mixture was taken into a double pipe heat exchanger to decrease the bulk temperature of the gas mixture as soon as it leaves the reactor (Figure 2.2). Tap water flowed in the outer pipe and hot gas mixture passed through the inner pipe. The heat exchanger was manufactured from stainless steel. A Cu-Constantan thermocouple, which was connected to a digital temperature reader, was placed at the exit of heat exchanger to monitor the outlet heat exchanger temperature of gas mixture. The temperature profile along the heat exchanger was predicted as shown in Appendix B. It was estimated that the temperature of the gas mixture can be reduced from 400°C to 30°C within about 10cm. Heat exchanger and the furnace are the most important part of the experimental set-up. The accuracy of the experimental data is dependent on the diligent operation of these two apparatus. After the cooling, the gas mixture enters to the Fourier Transform Infrared spectrophotometer to perform the chemical analysis. FT-IR is linked to a computer. By the help of the computer, the spectra of the gas mixture were obtained and recorded.

The volumetric flow rates of gases in the experiment were adjusted by mass flow controllers (Figure 2.3). At the inlet streams of the mass flow controllers, there are two needle valves to adjust the flow rates of gases in the range of the mass flow

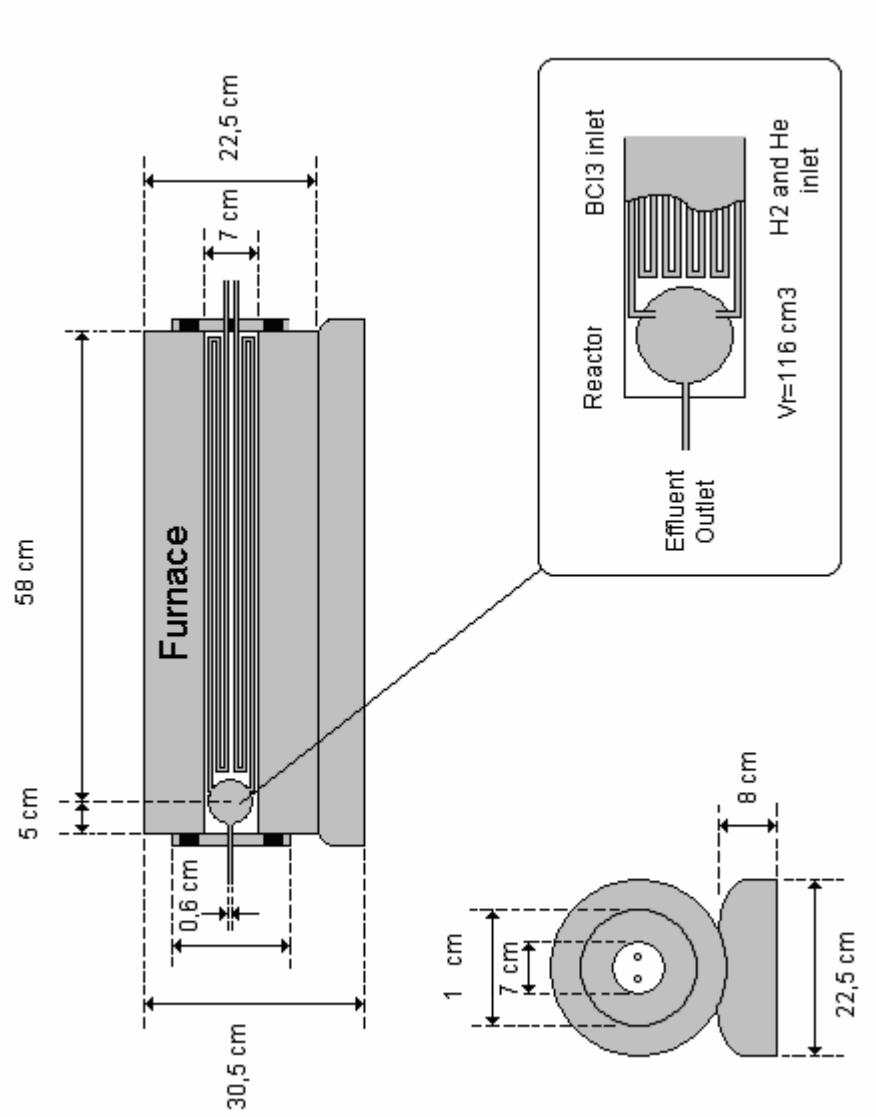


Figure 2.1. Schematic Diagram of Reactor and Furnace

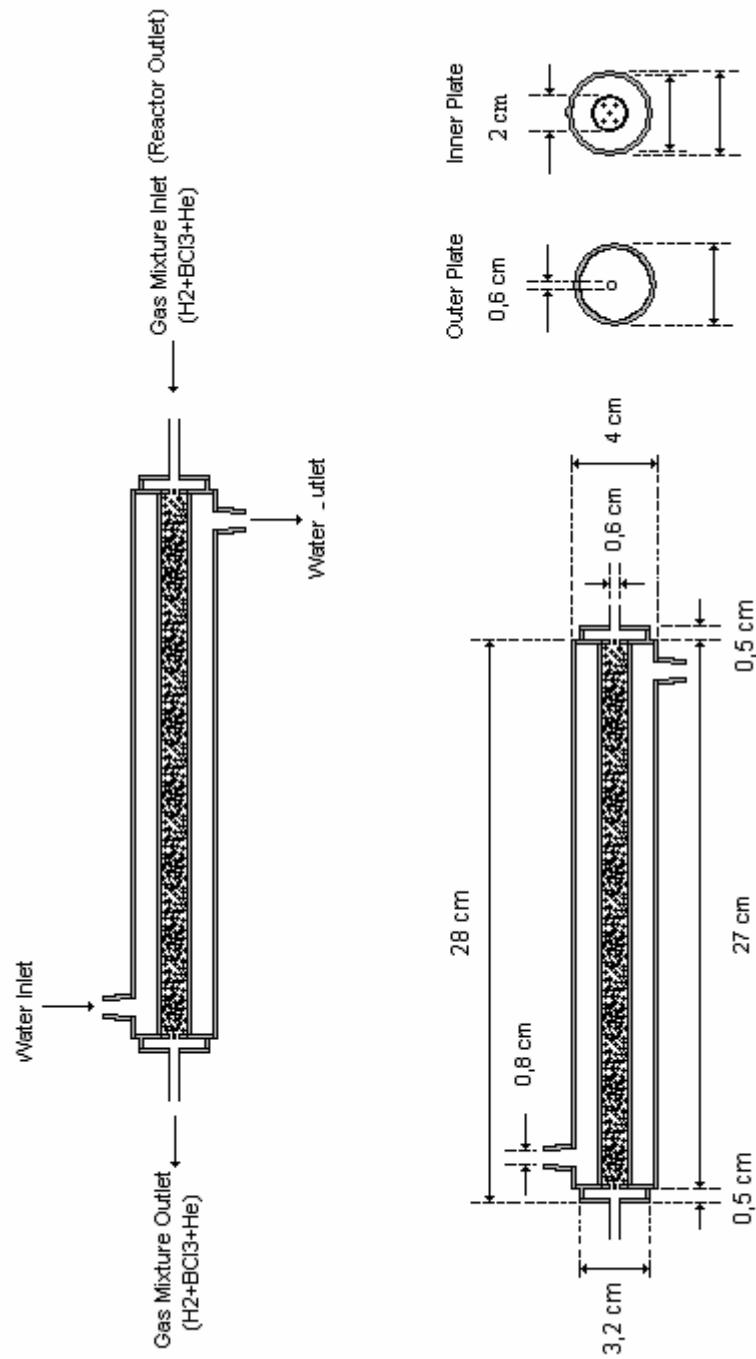


Figure 2.2. Heat Exchanger

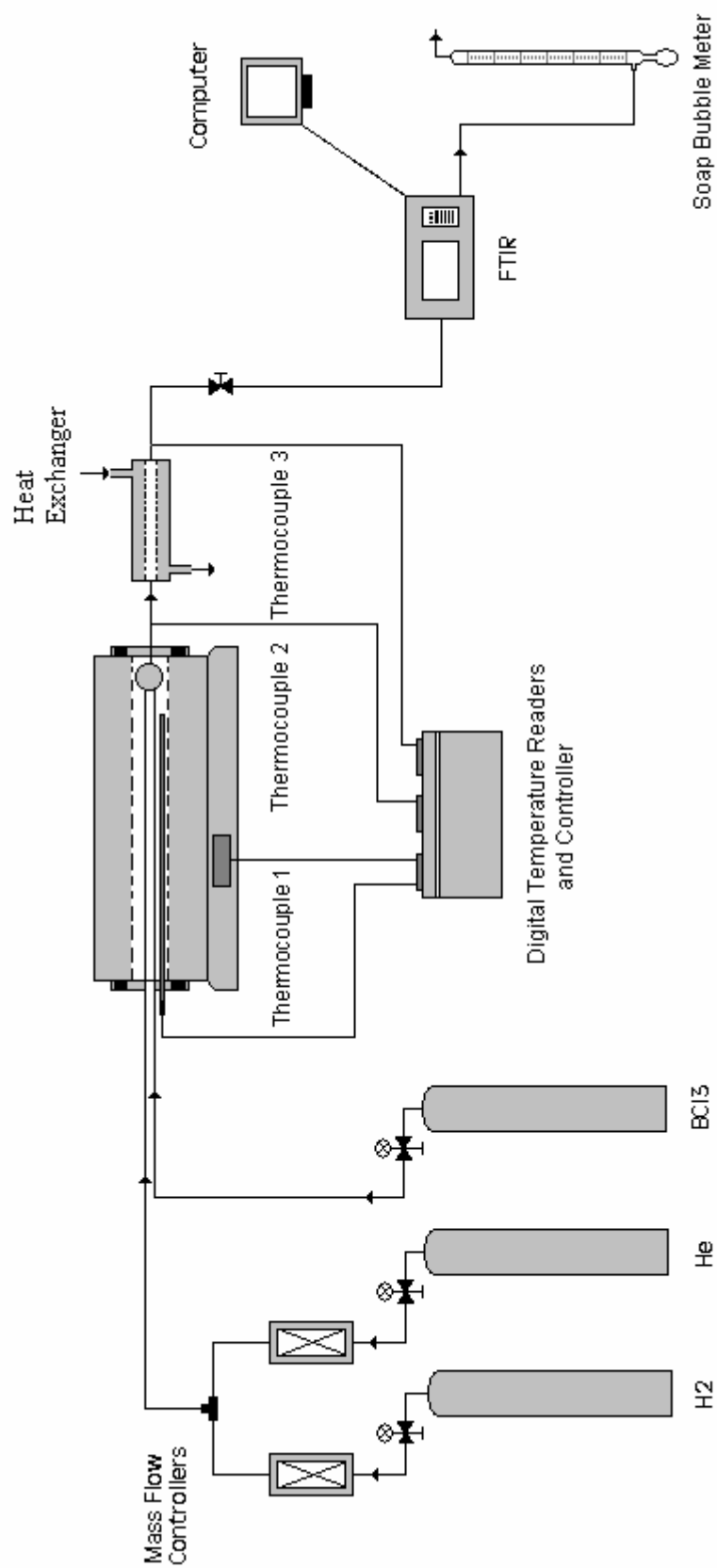


Figure 2.3. Schematic Diagram of Experimental Set-up

controller roughly. Also two filters were located to prevent the impurities coming from the gas tubes before entering the controllers. The impurities can affect the accuracy of mass flow controllers; also they can damage the mass flow controllers. The mass flow controllers have a range of 0-500 ml/min for the gas flow of hydrogen and helium.

In the experiment, three gases were used. These are helium, hydrogen and boron trichloride. The pressures of the gases were adjusted by the pressure regulator installed at the top of the gas tubes. A soap bubble meter was placed at the exit of the FTIR to compare the apparent flow rate of gases with the mass flow controller reading values. The exit of the soap bubble meter was discarded to the atmosphere. Because BCl_3 is a toxic gas and H_2 is inflammable; the furnace was placed under a hood made of stainless steel. This hood was used to prevent the harmful effects of BCl_3 and H_2 at the possibility of the gas leakage. This hood completely surrounds the furnace. A ventilation system connected to the hood was used during the experiment. Since the condensation temperature of BCl_3 at 1 bar is 15°C , heating tape was used on the line between the reactor inlet and the BCl_3 gas tube. This tape prevents the condensation of BCl_3 in the pipe.

2.2. Experimental Procedure

The experiments were carried out at a gauge pressure of 1 bar with a total volumetric flow rate of $200 \times 10^{-6} \text{ m}^3/\text{min}$. As it is mentioned above, there are three gases used in the experiments. BCl_3 and H_2 were the reactant gases. In addition to these gases, helium was used to purge the experimental set-up before and after each experiment, and as diluents in the experimental set-up.

The experimental procedure can be divided into three parts. The first one is the calibration experiment. The second one is the $\text{BCl}_3\text{-H}_2$ experiments in which the mole fraction of BCl_3 was changed in each set of experiment. The third one is the $\text{BCl}_3\text{-H}_2\text{-He}$ experiments in which the mole fraction of BCl_3 was kept constant and mole fraction of H_2 in the reactant gas mixture was changed. The experimental conditions for the last two experiment groups were the same and not changed except reactant mole fractions. The results of last two experiments were evaluated together and used to deduce the gas phase reaction kinetic.

In the calibration experiments, reactants were passed through FT-IR with a gas cell temperature of 110°C . The chemical analysis of the reactants was performed by using FT-IR. The FT-IR spectra for known compositions were used to obtain the calibration curve. Calibration curves of boron trichloride and hydrochloric acid were drawn by using these spectra. Calibration methods are given in Appendix A.

In the kinetic experiments, before starting, the gas cell was heated up to 110°C to prevent the condensation of BCl_3 in the effluent stream. The flow rates of BCl_3 and H_2 were adjusted before the reactor was heated. After the reactor temperature reached its desired value, the FT-IR spectra were taken until the reactor reaches its steady state. The gas phase reaction takes place in the CSTR which was placed in the furnace. Hereafter, the gas stream was quenched by passing through the heat exchanger to stop the gas phase reaction. The temperature of the gas stream was continuously measured by the thermocouple placed at the exit stream of the heat exchanger. When the temperature did not drop to a low value, the flow rate of tap water was increased. Then heat exchanger outlet gas stream enters the gas cell of the FT-IR. Finally, the gas mixture was vented out to the atmosphere after the analyzed gas mixture was passed through the soap bubble meter. This procedure was applied

for various temperatures of reactor and for different inlet compositions of BCl_3 . The operation conditions of the experiments are given in the following tables. At the end of the each experiment, the experimental set-up was purged to remove the unreacted gases from the system. The experimental conditions are shown in Table 2.1 to Table 2.11.

Table 2.1. Experimental Conditions for BCl₃-H₂ Experiments (Tot. Vol. Flowrate: 209.07 ml/min, y_{BCl₃o}=0.025 and y_{H₂o}=0.975)

Run Number	t (min)	T _s (°C)	T _f (°C)	T _r (°C)	T _e (°C)
BCI3-1-65	35	330	336.9	267	31.4
BCI3-1-57	35	390	397.0	317	32.3
BCI3-1-49	40	435	441.9	356	33.2
BCI3-1-42	40	480	485.9	395	34.9
BCI3-1-33	30	523	528.5	437	35.4
BCI3-1-24	35	580	585.4	490	36.8
BCI3-1-16	35	630	635.0	538	38.4

Table 2.2. Experimental Conditions for BCl₃-H₂ Experiments (Tot. Vol. Flowrate: 211.02 ml/min, y_{BCl₃o}=0.034 and y_{H₂o}=0.966)

Run Number	t (min)	T _s (°C)	T _f (°C)	T _r (°C)	T _e (°C)
BCI3-2-64	35	330	335.2	267	32.0
BCI3-2-57	35	390	396.7	317	32.6
BCI3-2-49	40	435	440.8	356	33.7
BCI3-2-42	40	480	485.5	395	33.9
BCI3-2-33	30	523	529.1	437	34.6
BCI3-2-24	35	580	585.6	490	35.0
BCI3-2-16	30	630	635.2	538	36.4

Table 2.3. Experimental Conditions for BCl₃-H₂ Experiments (Tot. Vol. Flowrate: 213.62 ml/min, y_{BCl₃o}=0.046 and y_{H₂o}=0.954)

Run Number	t (min)	T _s (°C)	T _f (°C)	T _r (°C)	T _e (°C)
BCI3-3-64	35	330	336.7	267	29.7
BCI3-3-57	35	390	396.8	317	31.5
BCI3-3-49	40	435	441.4	356	32.1
BCI3-3-42	40	480	485.8	395	33.0
BCI3-3-33	30	523	528.7	437	33.9
BCI3-3-24	35	580	585.4	490	34.8
BCI3-3-16	30	630	634.8	538	36.1

Table 2.4. Experimental Conditions for BCl₃-H₂ Experiments (Tot. Vol.**Flowrate: 215.7 ml/min, $y_{\text{BCl}_3_0}=0.058$ and $y_{\text{H}_2_0}=0.942$)**

Run Number	t (min)	T _s (°C)	T _f (°C)	T _r (°C)	T _e (°C)
BCI3-4-64	35	330	335.0	267	32.0
BCI3-4-57	35	390	395.8	317	33.0
BCI3-4-49	40	435	441.8	356	33.6
BCI3-4-42	40	480	485.5	395	34.3
BCI3-4-33	30	523	528.6	437	35.8
BCI3-4-24	35	580	586.0	490	36.2
BCI3-4-16	30	630	635.8	538	37.5

Table 2.5. Experimental Conditions for BCl₃-H₂-He Experiments (Tot. Vol.**Flowrate: 207.18 ml/min, $y_{\text{BCl}_3_0}=0.066$, $y_{\text{H}_2_0}=0.086$ and $y_{\text{He}}=0.848$)**

Run Number	t (min)	T _s (°C)	T _f (°C)	T _r (°C)	T _e (°C)
H2-15-65	35	330	336.7	262	31.2
H2-15-57	35	390	396.8	317	32.1
H2-15-49	40	435	440.5	354	33.0
H2-15-42	40	480	485.7	394	34.2
H2-15-33	30	523	528.5	433	34.8
H2-15-24	35	580	585.4	490	35.2
H2-15-16	35	630	634.5	535	36.4

Table 2.6. Experimental Conditions for BCl₃-H₂-He Experiments (Tot. Vol.**Flowrate: 207.25ml/min, $y_{\text{BCl}_3_0}=0.066$, $y_{\text{H}_2_0}=0.115$ and $y_{\text{He}}=0.819$)**

Run Number	t (min)	T _s (°C)	T _f (°C)	T _r (°C)	T _e (°C)
H2-20-65	35	330	335.8	262	33.4
H2-20-57	35	390	397.0	317	33.0
H2-20-49	40	435	440.8	354	33.6
H2-20-42	40	480	485.9	394	34.8
H2-20-33	30	523	528.5	433	35.4
H2-20-24	35	580	585.5	490	36.8
H2-20-16	35	630	634.5	535	38.1

Table 2.7. Experimental Conditions for BCl₃-H₂-He Experiments (Tot. Vol.**Flowrate: 207.31ml/min, $y_{\text{BCl}_3_0}$ =0.066, $y_{\text{H}_2_0}$ =0.143 and y_{He} =0.791)**

Run Number	t (min)	T _s (°C)	T _f (°C)	T _r (°C)	T _e (°C)
H2-25-65	35	330	335.2	262	30.5
H2-25-57	35	390	397.4	317	31.1
H2-25-49	40	435	441.6	354	31.9
H2-25-42	40	480	485.6	394	32.8
H2-25-33	30	523	529.0	433	33.5
H2-25-24	35	580	585.4	490	34.9
H2-25-16	35	630	636.0	535	36.2

Table 2.8. Experimental Conditions for BCl₃-H₂-He Experiments (Tot. Vol.**Flowrate: 207.38 ml/min, $y_{\text{BCl}_3_0}$ =0.066, $y_{\text{H}_2_0}$ =0.172 and y_{He} =0.762)**

Run Number	t (min)	T _s (°C)	T _f (°C)	T _r (°C)	T _e (°C)
H2-30-65	35	330	335.1	262	31.4
H2-30-57	35	390	396.2	317	32.2
H2-30-49	40	435	440.9	354	33.6
H2-30-42	40	480	486.1	394	34.4
H2-30-33	30	523	529.2	433	35.5
H2-30-24	35	580	585.6	490	36.9
H2-30-16	35	630	635.9	535	37.8

Table 2.9. Experimental Conditions for BCl₃-H₂-He Experiments (Tot. Vol.**Flowrate: 207.44 ml/min, $y_{\text{BCl}_3_0}$ =0.066, $y_{\text{H}_2_0}$ =0.200 and y_{He} =0.734)**

Run Number	t (min)	T _s (°C)	T _f (°C)	T _r (°C)	T _e (°C)
H2-35-65	35	330	335.8	262	33.5
H2-35-57	35	390	395.8	317	33.9
H2-35-49	40	435	441.0	354	34.6
H2-35-42	40	480	486.4	394	35.8
H2-35-33	30	523	529.3	433	36.9
H2-35-24	35	580	586.0	490	37.8
H2-35-16	35	630	634.9	535	39.2

Table 2.10. Experimental Conditions for BCl₃-H₂-He Experiments (Tot. Vol.**Flowrate: 207.52 ml/min, $y_{\text{BCl}_3_0}=0.066$, $y_{\text{H}_2_0}=0.228$ and $y_{\text{He}}=0.706$)**

Run Number	t (min)	T _s (°C)	T _f (°C)	T _r (°C)	T _e (°C)
H2-40-65	35	330	335.2	262	31.8
H2-40-57	35	390	396.0	317	32.6
H2-40-49	40	435	440.5	354	33.4
H2-40-42	40	480	486.1	394	34.2
H2-40-33	30	523	529.1	433	35.0
H2-40-24	35	580	585.5	490	36.2
H2-40-16	35	630	636.0	535	37.5

Table 2.11. Experimental Conditions for Reproducibility of Experiment BCl₃-4**(Tot. Vol. Flowrate: 218.2 ml/min, $y_{\text{BCl}_3_0}=0.065$ and $y_{\text{H}_2_0}=0.938$)**

Run Number	t (min)	T _s (°C)	T _f (°C)	T _r (°C)	T _e (°C)
ReproBCl3-4-65	35	330	336.5	266	32.3
ReproBCl3-4-57	35	390	396.3	315	33.0
ReproBCl3-4-49	30	435	441.1	352	34.2
ReproBCl3-4-42	40	480	485.8	393	36.3
ReproBCl3-4-33	40	523	528.7	435	38.0
ReproBCl3-4-24	35	580	585.2	490	39.5
ReproBCl3-4-16	35	630	634.9	535	40.4

CHAPTER 3

RESULTS AND DISCUSSION

3.1 Chemical Analysis of Reactant Outlet Stream

The data necessary to determine the gas phase reaction kinetics were obtained using the FTIR spectra of the outlet gas mixture. Concentrations of the gas phase products and reactants were monitored online during the experiments. The FTIR spectrum contains the peaks of HCl and BHCl_2 and BCl_3 . At first sight, these peaks give qualitative information about the reaction medium. By using the calibration curves for HCl and BCl_3 , which are given in Appendix A, the chemical composition of reactor inlet and outlet streams were evaluated. In other words, quantitative information about the gas phase reaction was obtained. The spectra of outlet gas mixture before and after heating the reactor are given in Figure 3.1 and Figure 3.2, respectively. For the calculation of conversion and reaction rate, HCl peak was used. The reason for taking the HCl peak is the fidelity of this peak. In the experiment, BCl_3 was manually controlled. Reaction product, BHCl_2 does not have calibration curve and it is calibrated by using the mole fraction of HCl in the gas stream.

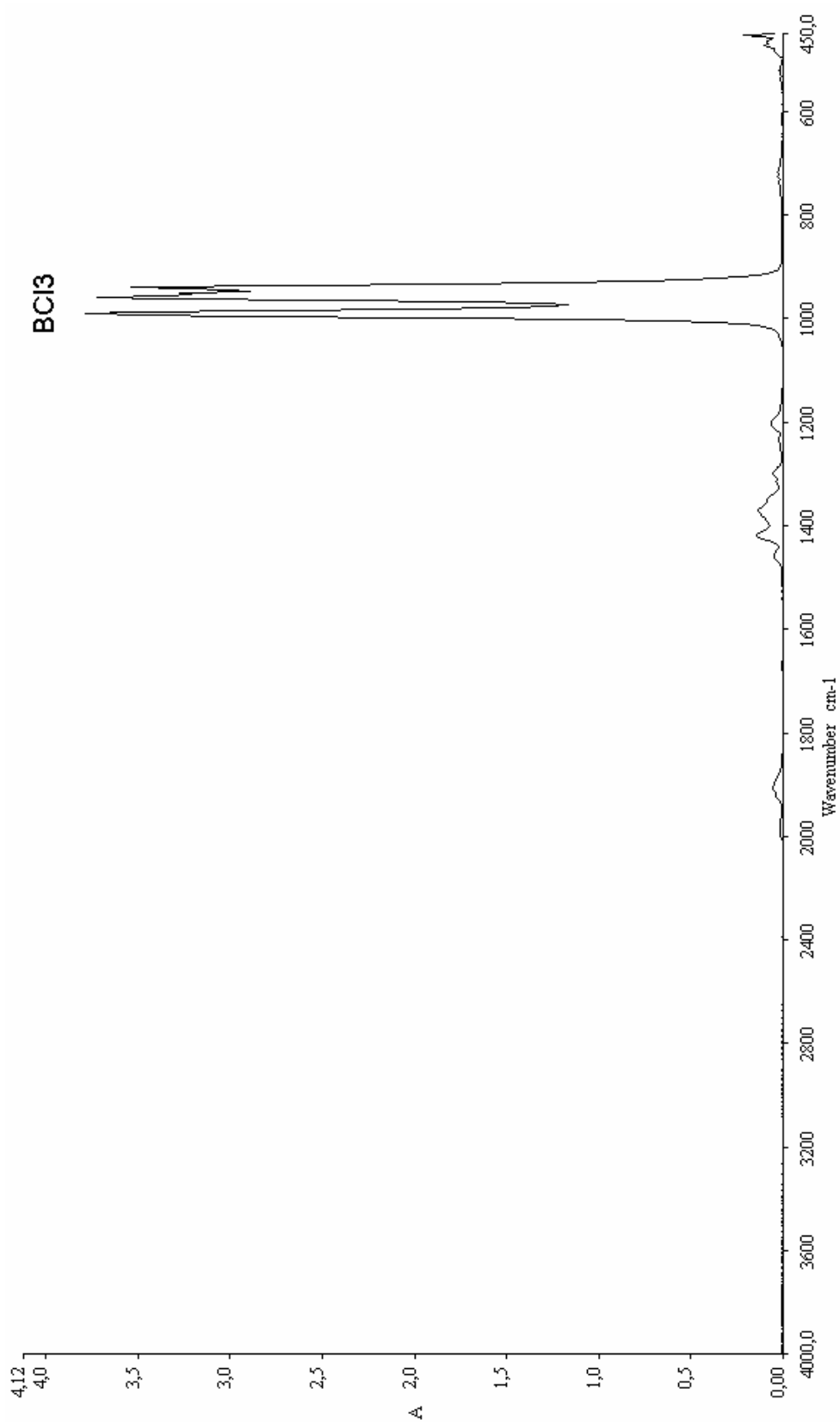


Figure 3.1 FTIR Spectrum of Gas Mixture before Heating the Reactor

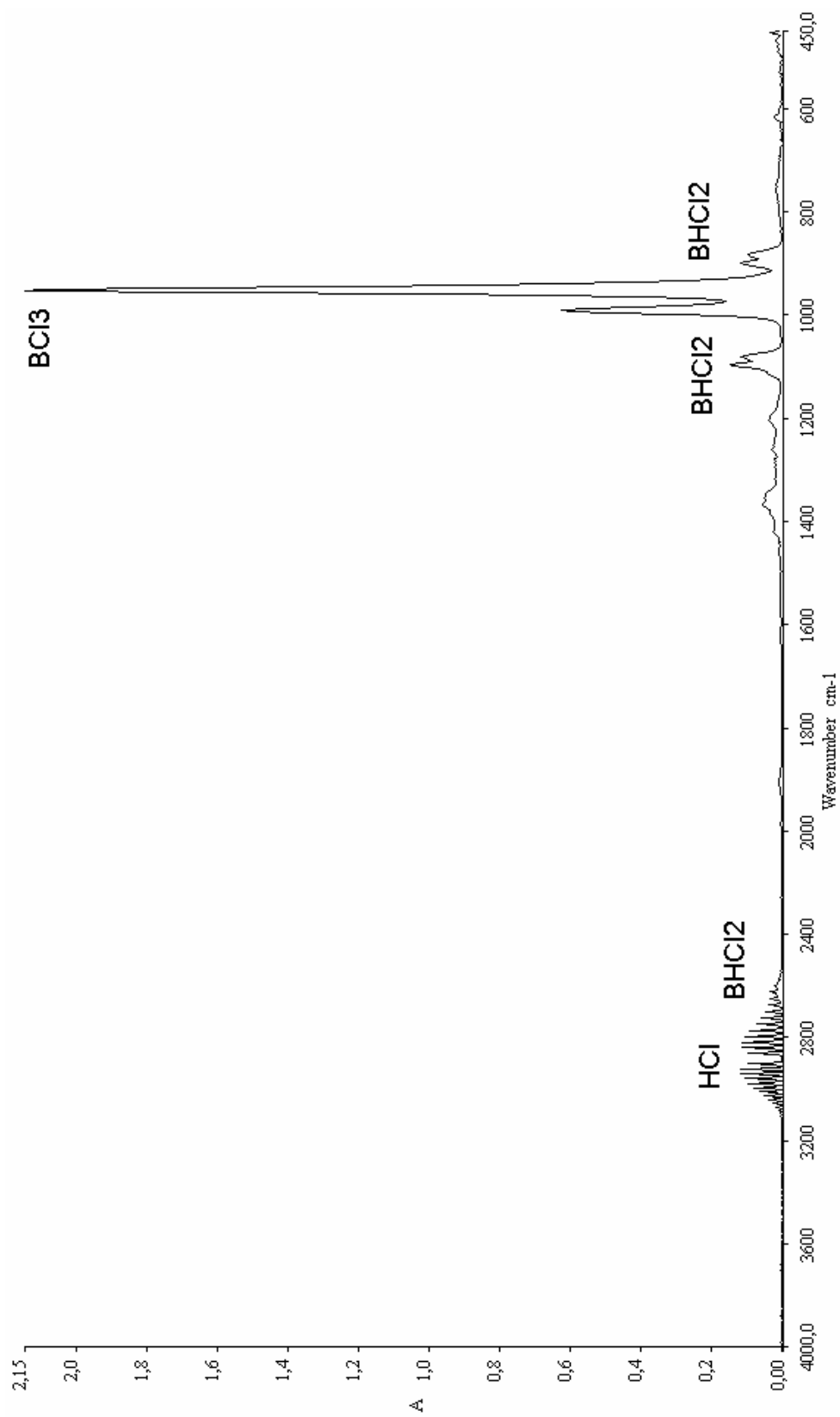


Figure 3.2 FTIR Spectrum of Gas Mixture after Heating the Reactor

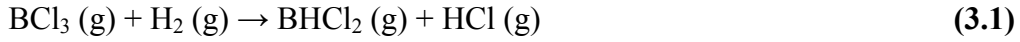
HCl gives its characteristic peaks at wavenumbers between 2700 cm^{-1} and 3050 cm^{-1} . BCl_3 peak is at wavenumbers between 900 and 1050 cm^{-1} and BHCl_2 has three characteristic peaks. Two of them are near the peak of BCl_3 and the other are near the peak of HCl. The wavenumbers of these peaks are 850-910 cm^{-1} , 1050-1150 cm^{-1} and 2625-2700 cm^{-1} , respectively. These results are consistent with the previous study of Sezgi (1997).

As it is mentioned before, the experiments are divided into two main groups. First set of experiments includes the data obtained for the case in which mole fraction of BCl_3 was changed and mole fraction of H_2 was kept constant. In the second set, while mole fraction of BCl_3 was kept constant, mole fraction of H_2 and He were changed in each experiment. These experiment sets are necessary to determine the orders with respect to BCl_3 and H_2 concentrations in the rate expression. These two sets were combined and used to evaluate the rate expression of the gas phase reaction.

3.2 Reaction Rate of Each Species and the Conversion of Gas Phase Reaction

There are three independent variables and one dependent variable in the experiments. Independent variables are inlet gas composition, volumetric flow rate of gas mixture and temperature of the reactor. Dependent variable is the outlet gas composition. Thus, the raw data in Appendix C were obtained for different compositions of H_2 and BCl_3 at different reactor temperatures. The FT-IR spectra of the reactor outlet stream include only peaks of reactant BCl_3 and reaction products, BHCl_2 and HCl. Any intermediate product was not observed. The mole fractions of each component in the inlet and outlet streams are given in Appendix C. The

chemical species involved in the reaction system are BCl_3 , H_2 , HCl and BHCl_2 . There are three elements: B, Cl and H. One independent reaction is enough to describe the reaction system. The gas phase reaction is;



Four mole balance equations can be written for H_2 , BCl_3 , HCl and BHCl_2 (Eqn. 3.2-3.5). The molar flow rate and the total concentration of gas mixture were evaluated by using the ideal gas law. Here the limiting reactant is BCl_3 and that is why, conversion is determined by considering inlet mole fraction of BCl_3 .

$$F_{\text{BCl}_3} = F_{\text{BCl}_3^o} \cdot (1 - x) \quad (3.2)$$

$$F_{\text{H}_2} = F_{\text{H}_2^o} - F_{\text{BCl}_3^o} \cdot x = F_{\text{H}_2^o} \cdot \left(1 - \frac{F_{\text{BCl}_3^o}}{F_{\text{H}_2^o}} \cdot x\right) \quad (3.3)$$

$$F_{\text{BHCl}_2} = F_{\text{BCl}_3^o} \cdot x \quad (3.4)$$

$$F_{\text{HCl}} = F_{\text{BCl}_3^o} \cdot x \quad (3.5)$$

$$F_T = F_{\text{BCl}_3^o} + F_{\text{H}_2} = F_o \quad (3.6)$$

The outlet molar flow rates of each species are defined above in terms of conversion and inlet mole fraction of reactants. Now, outlet mole fractions of species are defined in terms of outlet molar flow rate. The total molar flow rate of gas mixture is calculated by using ideal gas equation. The molar flow rate of hydrogen chloride is equal to molar flow rate of dichloroborane because the same amount of HCl and BHCl_2 are produced in the gas phase reaction. Also, total molar flow rate of outlet gas mixture is equal to the total inlet molar flow rate and defined in Eqn. 3.6.

As seen from the reaction stoichiometry, there is not any volume change in the reaction system. That is why; the total outlet volumetric flow rate is taken equal to the inlet volumetric flow rate in the calculations. Here, F and x denote the molar flow rates of species and the conversion in the reaction system. The outlet mole fractions are;

$$y_{BCl_3} = \frac{F_{BCl_3}}{F_T} = \frac{F_{BCl_3o} \cdot (1-x)}{F_o} = y_{BCl_3o} \cdot (1-x) \quad (3.7)$$

$$y_{H_2} = \frac{(F_{H_2o} - F_{BCl_3o} \cdot x)}{F_o} = y_{H_2o} \cdot \left(1 - \frac{y_{BCl_3o}}{y_{H_2o}} \cdot x\right) \quad (3.8)$$

$$y_{BHCl_2} = \frac{F_{BHCl_2}}{F_o} = \frac{F_{BCl_3o} \cdot x}{F_o} = y_{BCl_3o} x \quad (3.9)$$

$$y_{HCl} = \frac{F_{HCl}}{F_o} = \frac{F_{BCl_3o} \cdot x}{F_o} = y_{BCl_3o} x \quad (3.10)$$

The conversion of boron trichloride can be calculated in terms of mole fractions in the effluent gas using Eqn 3.7 to 3.10. The outlet mole fractions are defined above. By using the outlet mole fractions and outlet molar flow rates, and the relations between the reaction rates were found (Eqn. 3.11). Knowing the conversion, reaction rates of different species were calculated using Eqn. 3.12 and Eqn. 3.13.

$$R_{BCl_3} = R_{H_2} = -R_{HCl} = -R_{BHCl_2} \quad (3.11)$$

$$R_{BCl_3} = R_{H_2} = -\frac{F_{BCl_3o} \cdot x}{V_R} = -\frac{F_o \cdot y_{BCl_3o} \cdot x}{V_R} \quad (3.12)$$

$$R_{BHCl_2} = R_{HCl} = \frac{F_{BCl_3o} \cdot x}{V_R} = \frac{F_o \cdot y_{BCl_3o} \cdot x}{V_R} \quad (3.13)$$

Here F_o denotes the initial molar flow rate of reactant gas mixture and it is calculated by using the ideal gas law. V_R is defined as the volume of reactor which is equal to $116 \times 10^{-6} \text{ m}^3$. The space time of reactants in the reactor was approximately 0.58 min. A continuous stirred reactor was selected to achieve homogeneous temperature distribution in the reactor. Also, the well mixing of the gases was supplied by fixing the pipes entering to the reactor face to face. The total volume from the exit of the reactor to heat exchanger is equal to $4.63 \times 10^{-6} \text{ m}^3$. This volume is very important because this part behaves as PFR and effects the reaction rate calculation. That is why; this volume was tried to be as small as possible. This value is negligible when compared to the volume of the reactor. Since the ratio of the volume between reactor and heat exchanger to the reactor, which is approximately 0.04, is low, this value was neglected in the calculations. The reaction rates of each species were evaluated using the Eqn. 3.11. Equation 3.14 is the reaction rate expression for the gas phase reaction. Activation energy of this reaction was calculated by using Eqn 3.15;

$$R_{BCl_3} = -k \cdot C_{BCl_3}^a \cdot C_{H_2}^b \quad (3.14)$$

$$k = k_o \cdot \exp\left[-\frac{E_a}{R \cdot T}\right] \quad (3.15)$$

Here a and b are the orders of BCl_3 and H_2 concentrations. E_a is the activation energy and k_o is the frequency factor. These parameters were calculated by using nonlinear regression program. 60 data points with different temperatures and the reactant concentrations were used in the calculation.

3.3 Reproducibility of the Experimental Data

The reproducibility experiment is important to test the reliability of the experimental data. In order to determine the reproducibility of the data, two experiments were performed and the results were compared. Change of HCl mole fraction in the reactor effluent stream as a function of temperature for these two runs is shown in Figure 3.3. Experimental results for HCl mole fraction consistent with each other. However, experimental results for BCl₃ mole fraction do not yield good agreement with each other (Figure 3.4). Knowing conversion, reactor outlet mole fractions of each component were calculated except HCl mole fraction. Conversion was calculated by dividing HCl mole fraction by initial mole fraction of BCl₃. Since the volumetric flow rate of BCl₃ was adjusted by the needle valve and it was very difficult to adjust the same flow rate. It was nearly impossible to find exactly the same result. The results of these two experiments are given in Table C.4 and Table C.11 in Appendix C and they are not the same. The initial mole fractions of BCl₃ in each experiment were 0.065 and 0.058. The difference in the mole fractions of BCl₃ makes the error getting higher.

3.4 Data Acquisition Method

Data acquisition is the one of the most important part of experiments. The experimental data must be reliable. This can only be provided by taking the data at steady state. During the experiment, the outlet mole fractions of BCl₃, HCl and BHCl₂ give clues about how well the steady state is achieved. The chemical analysis of the gas mixture was performed by considering the FT-IR spectra.

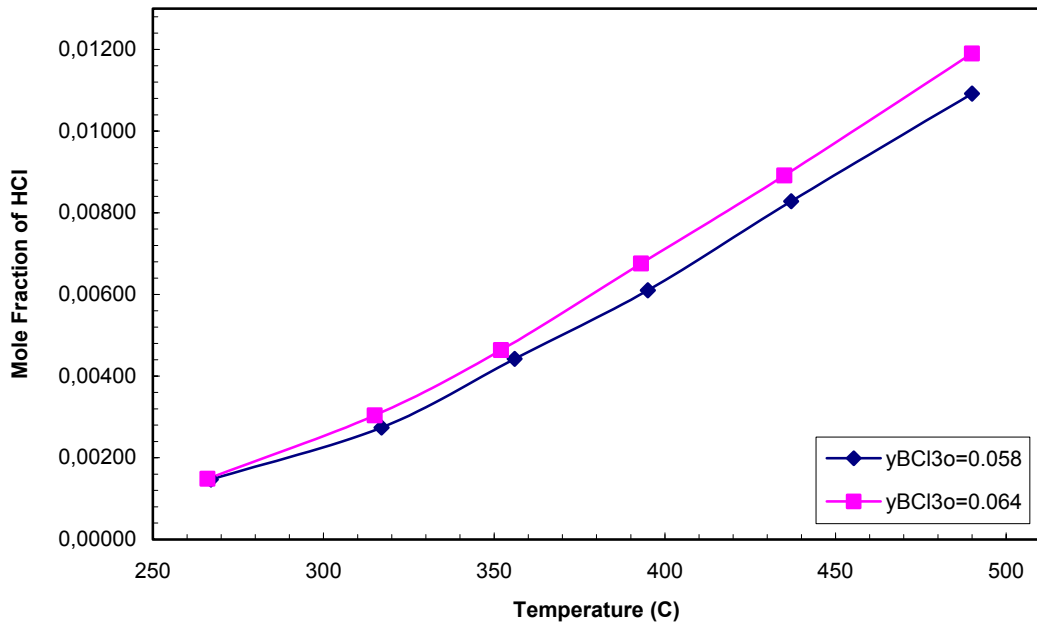


Figure 3.3 Change of HCl Mole Fraction in the Reactor Effluent Stream as a Function of Temperature

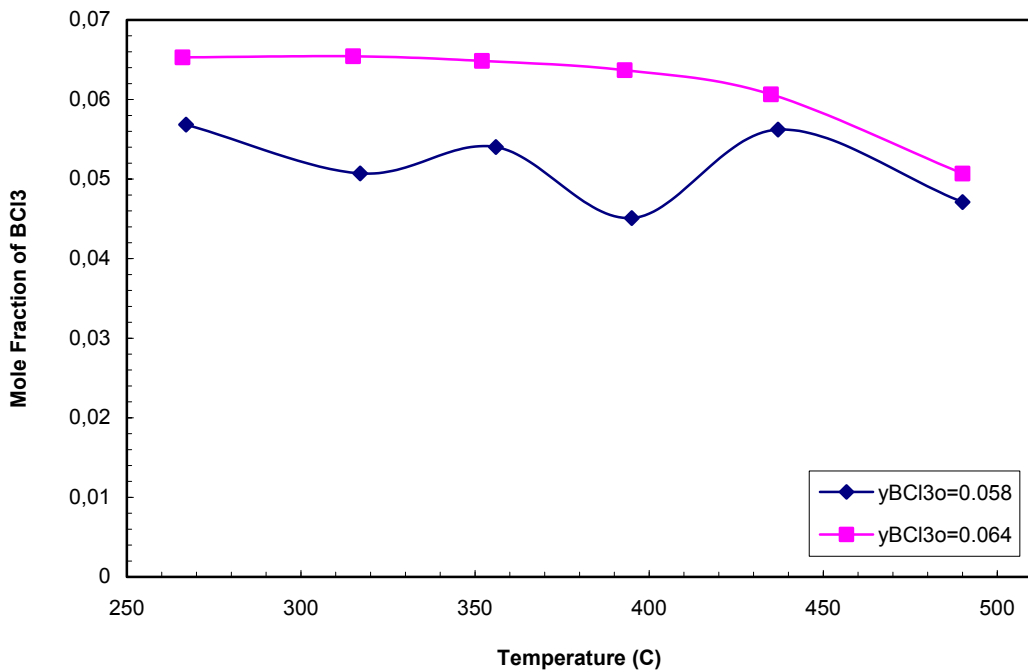


Figure 3.4 Change of BCl₃ Mole Fraction in the Reactor Effluent Stream as a Function of Temperature

The steady state mole fractions of BCl_3 , HCl and BHCl_2 are given in Figure 3.5. This figure shows that the system reaches the steady-state in a short time. The effluent gas composition indicated some fluctuations with time at the initial steps of reaction. These fluctuations are the results of change in reactor temperature during the heating or cooling process of the reactor.

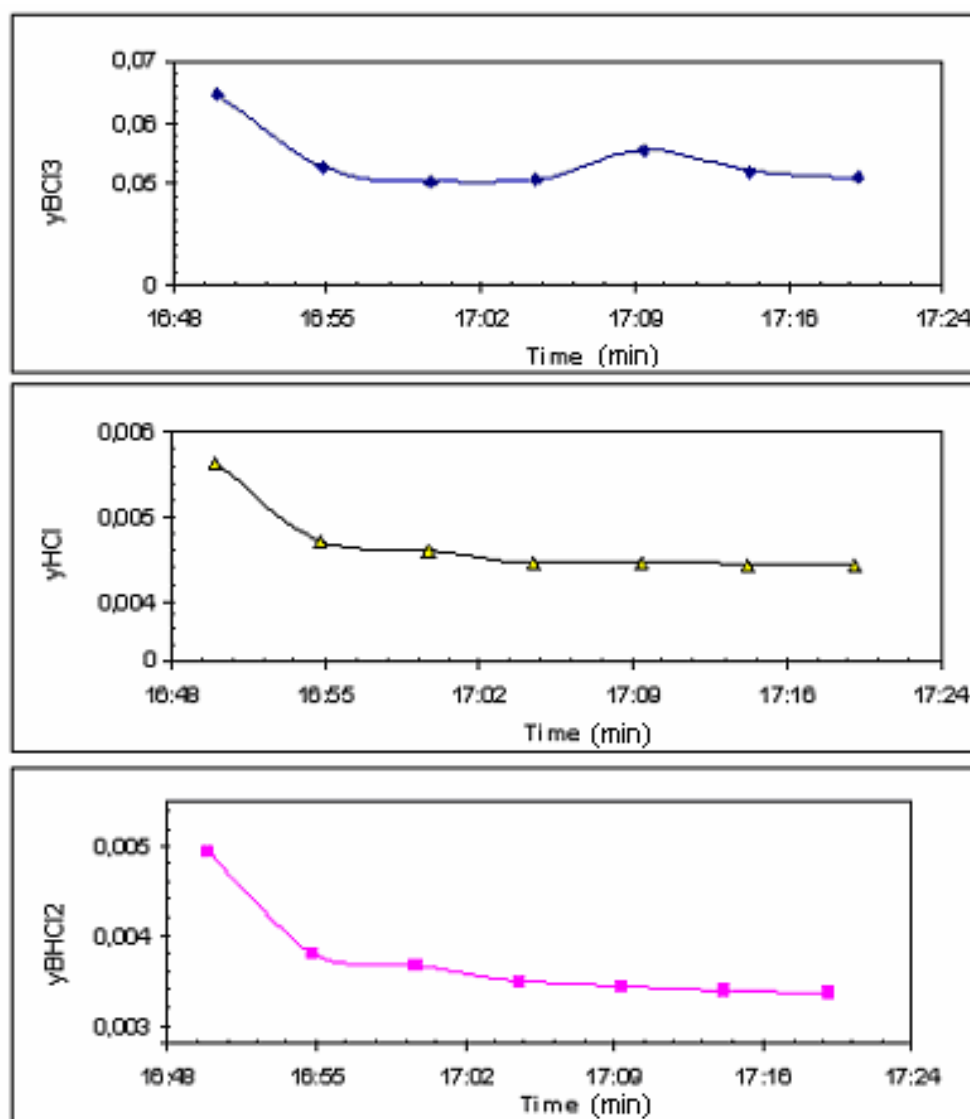


Figure 3.5 Steady State Outlet Mole Fractions of BCl_3 , HCl and BHCl_2 (Total Volumetric Flow Rate: 207.18 ml/min, $T_r=490^\circ\text{C}$, $y_{\text{BCl}_3_0}=0.066$, $y_{\text{H}_2}=0.086$, $y_{\text{He}}=0.848$)

3.5 Results for BCl₃-H₂ Experiments

In this part the mole fraction of BCl₃ was changed between 0.020 and 0.066 (See Appendix C). Experiments were carried at with four different inlet mole fractions of BCl₃ and different reactor temperatures. These experiments are essential for the determination of the order with respect to BCl₃ concentration in the reaction rate expression. The data analysis of the experiments is based on the determination of the reaction rate. The conversion was calculated using Eqn. 3.10. Mole fraction of HCl and inlet mole fraction of BCl₃ were used to calculate the conversion. Conversion is directly proportional with the exit mole fraction of HCl. On the other hand, it is inversely proportional with the inlet mole fraction of BCl₃. The molar flow rate of gas mixture was evaluated by using the ideal gas law. The outlet concentrations of the BCl₃ and H₂ were determined using the molar flow rates of gas mixture and conversion. Concentrations of reactants were used in the rate expression to simplify the calculations Eqn. 3.14. At first, the experimental reaction rate for each component was calculated from Eqn. 3.12 and Eqn. 3.13. Then, these values were used to determine the rate parameters in the proposed rate expression (Eqn. 3.14 and Eqn 3.15). These parameters are the orders with respect to H₂ and BCl₃ concentrations in the reaction rate, activation energy and the frequency factor.

It is observed that the conversion of BCl₃ to HCl decreases with an increase in the inlet mole fraction of BCl₃ in spite of the increase in the mole fraction of HCl in the effluent stream (Figure 3.6). The influence of temperature and initial mole fraction of BCl₃ on the conversion are shown in Figure 3.6. It shows that conversion increases with an increase in temperature. Effect of temperature on the mole fraction of BHCl₂ for different initial BCl₃ concentration is shown in Figure 3.8.

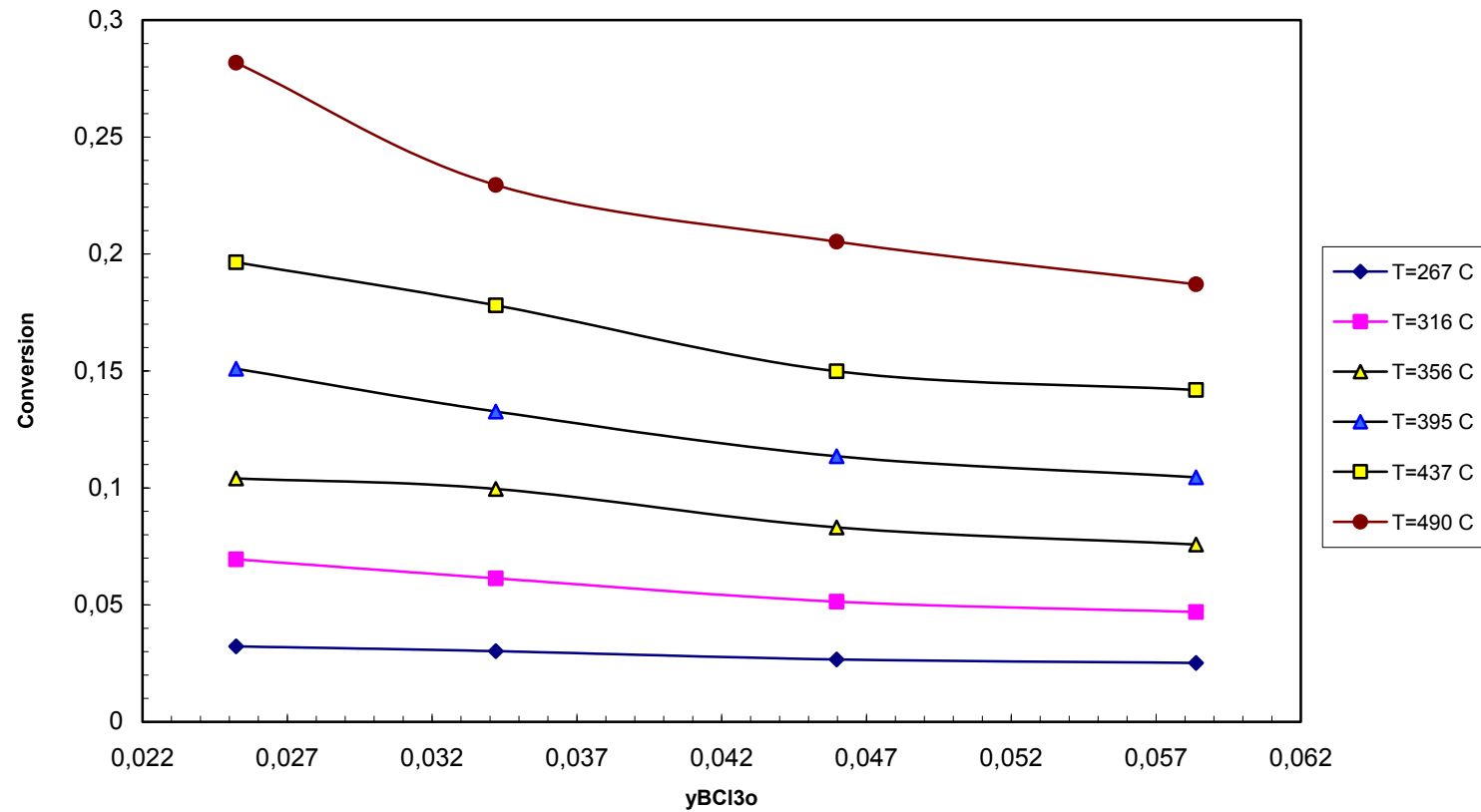


Figure 3.6 Effect of Initial Mole Fraction of BCl₃ on Conversion for Different Reactor Temperatures

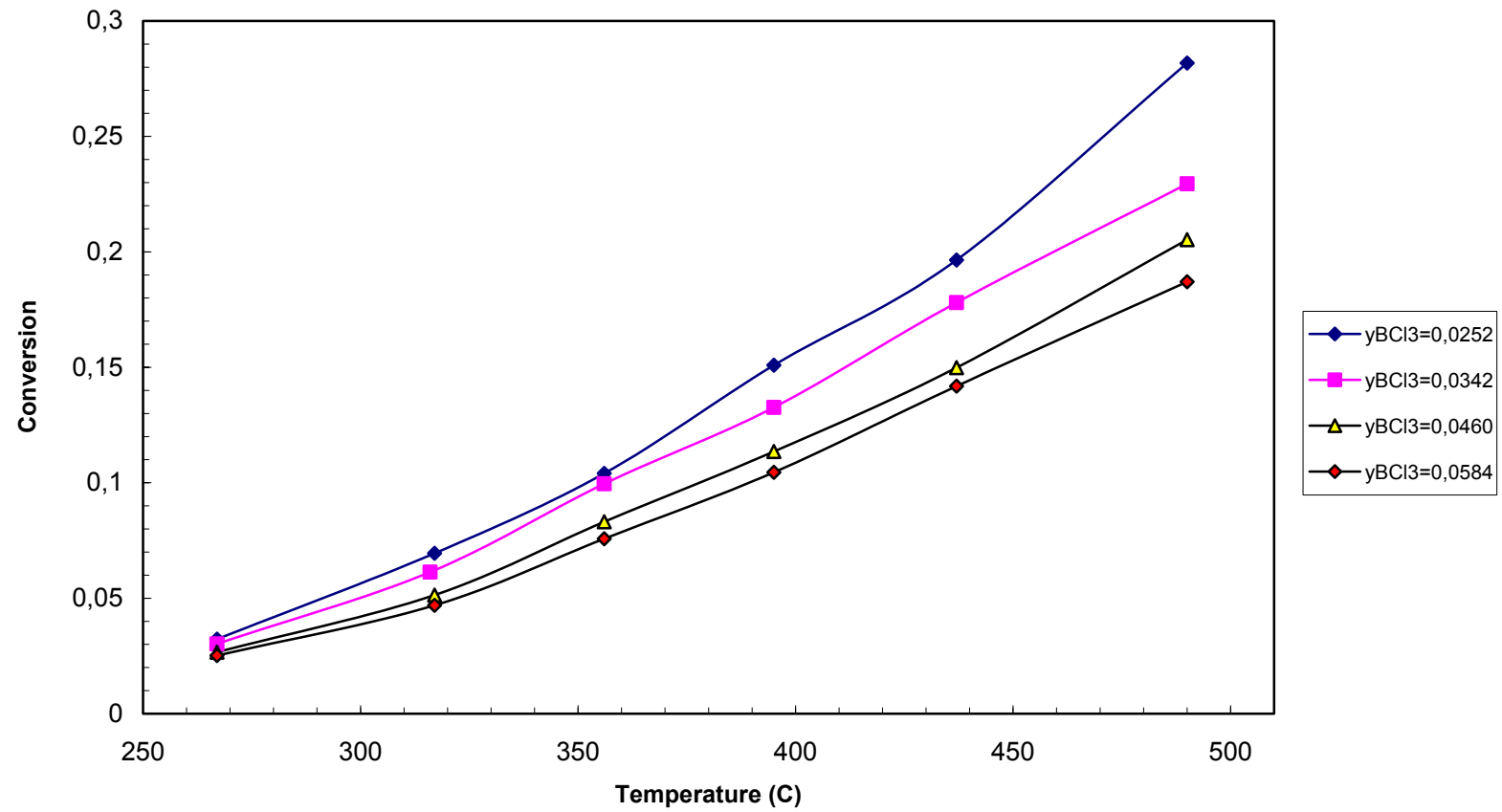


Figure 3.7 Effect of Temperature on Conversion for Different Inlet Compositions of BCl_3

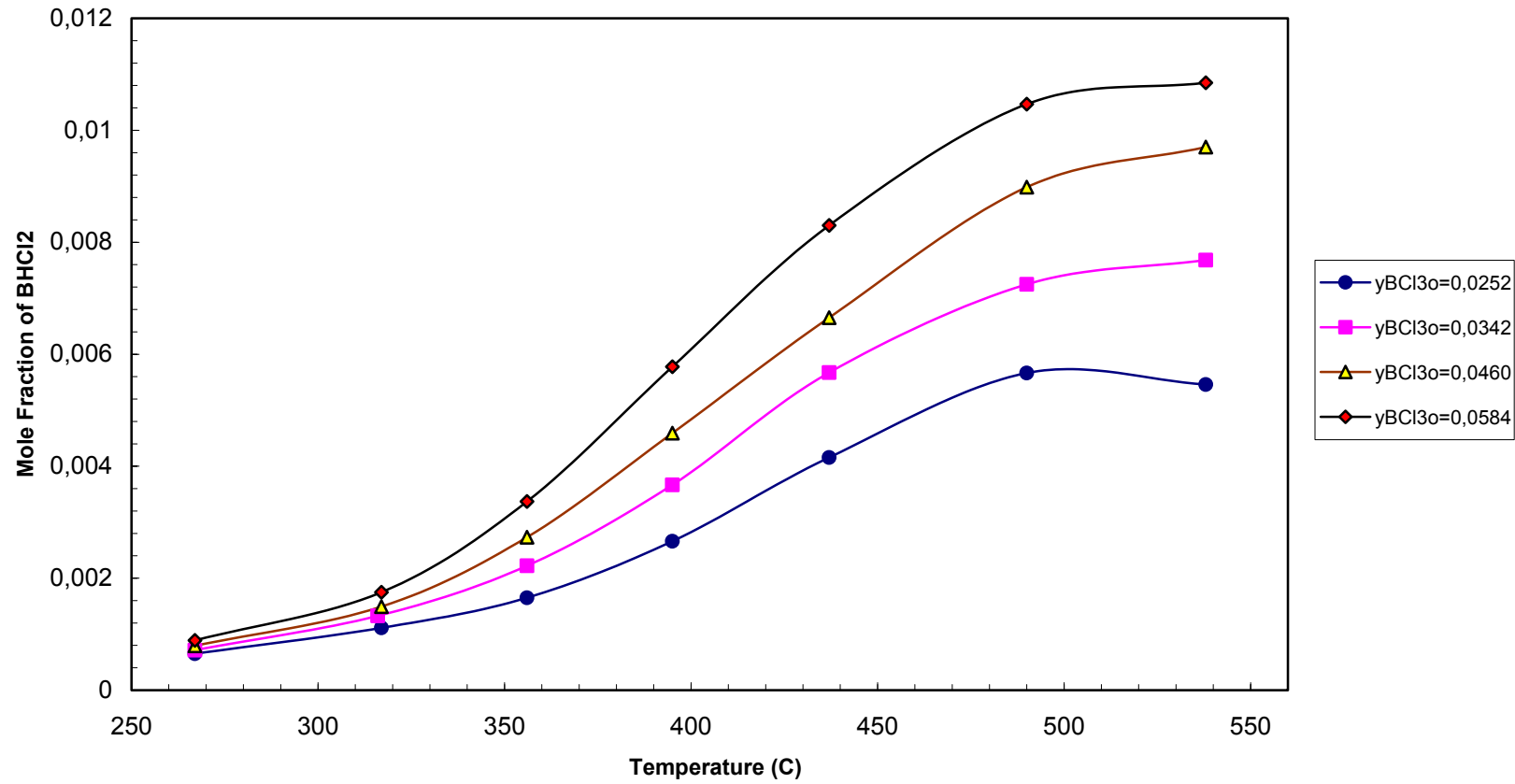
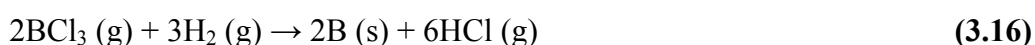


Figure 3.8 Effect of Temperature on Mole Fraction of BHCl_2 for Different Inlet Compositions of BCl_3

As it is seen from Figure 3.8, despite the increase in the mole fraction of HCl, mole fraction of BHCl₂ remains constant above a reactor temperature of 500°C. Surface reaction is the reason of this increase in HCl mole fraction because in the surface reaction three moles of HCl are produced for each mole of BCl₃ consumed. However in the gas phase reaction one mole of HCl is produced per mole of BCl₃ consumed. Surface reaction, boron formation, is given in Eqn. 3.16.



Since boron formation reaction was not considered in our calculations, the data above a temperature of 500°C were not used to find the rate parameters. Actually, mole fractions of HCl and BHCl₂ increase with an increase in reactor temperature, if there is not any surface reaction. Effect of temperature on the $\frac{y_{\text{BHCl}_2}}{y_{\text{HCl}}}$ ratio is shown in

Figure 3.9. As shown in this figure, the ratio remained constant at a value of one until a reactor temperature of 500°C. Above 500°C, this ratio decreased to 0.8. This result indicated that a surface reaction took place in the reactor above 500°C. Also at low reactor temperatures, the change in the mole fraction of HCl and conversion were in small amounts. That is why; the data at a reactor temperature of 262°C were not considered to find the rate parameters. These data affect the accuracy of the calculated data.

In Figure 3.10, effect of temperature on reaction rate of HCl is shown. Production rate of HCl in the reaction system increases with an increase in both reactor temperature and inlet mole fraction of BCl₃. Reaction rate of HCl was calculated using the Eqn. 3.13.

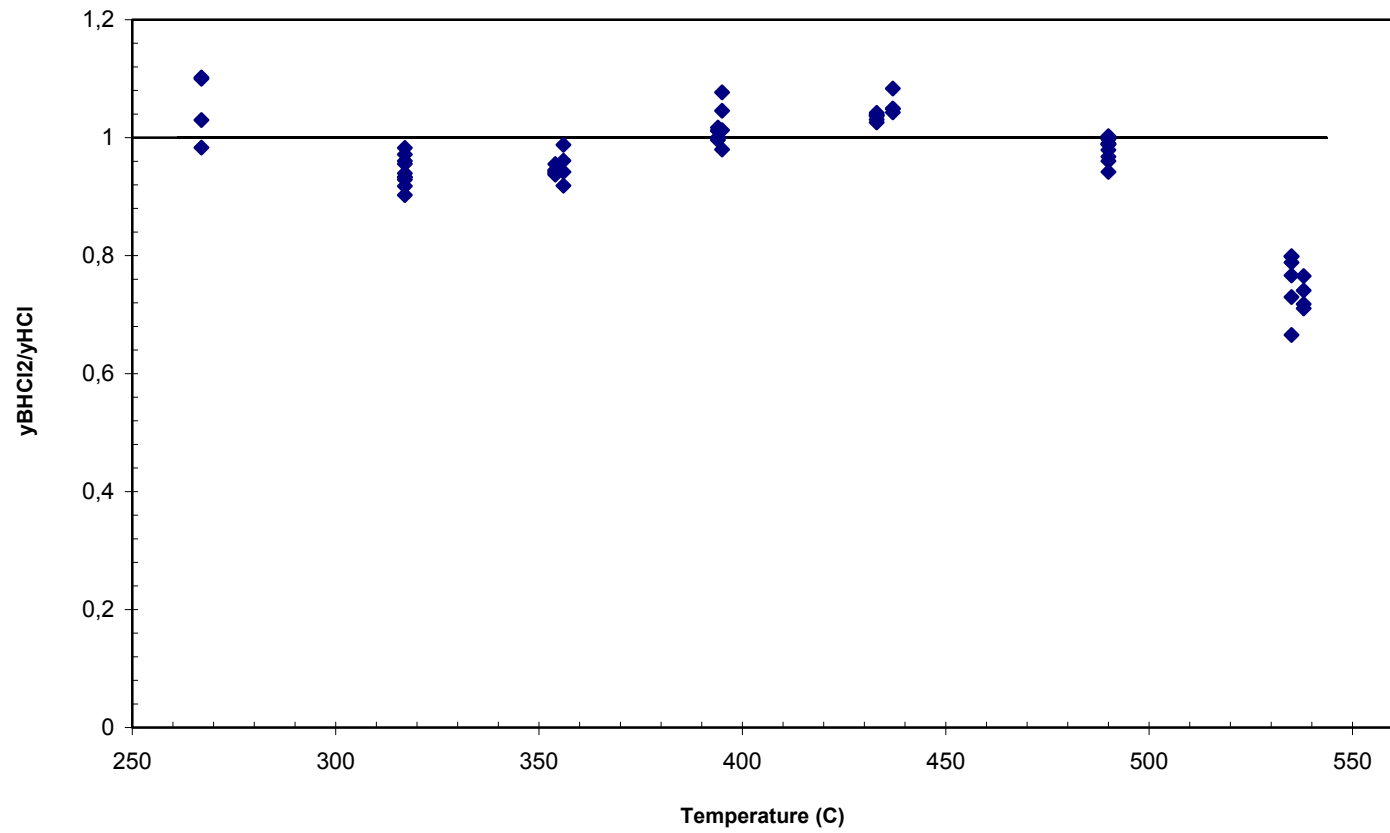


Figure 3.9 Effect of Temperature on the Ratio of BHCl_2 Mole Fraction to the HCl Mole Fraction

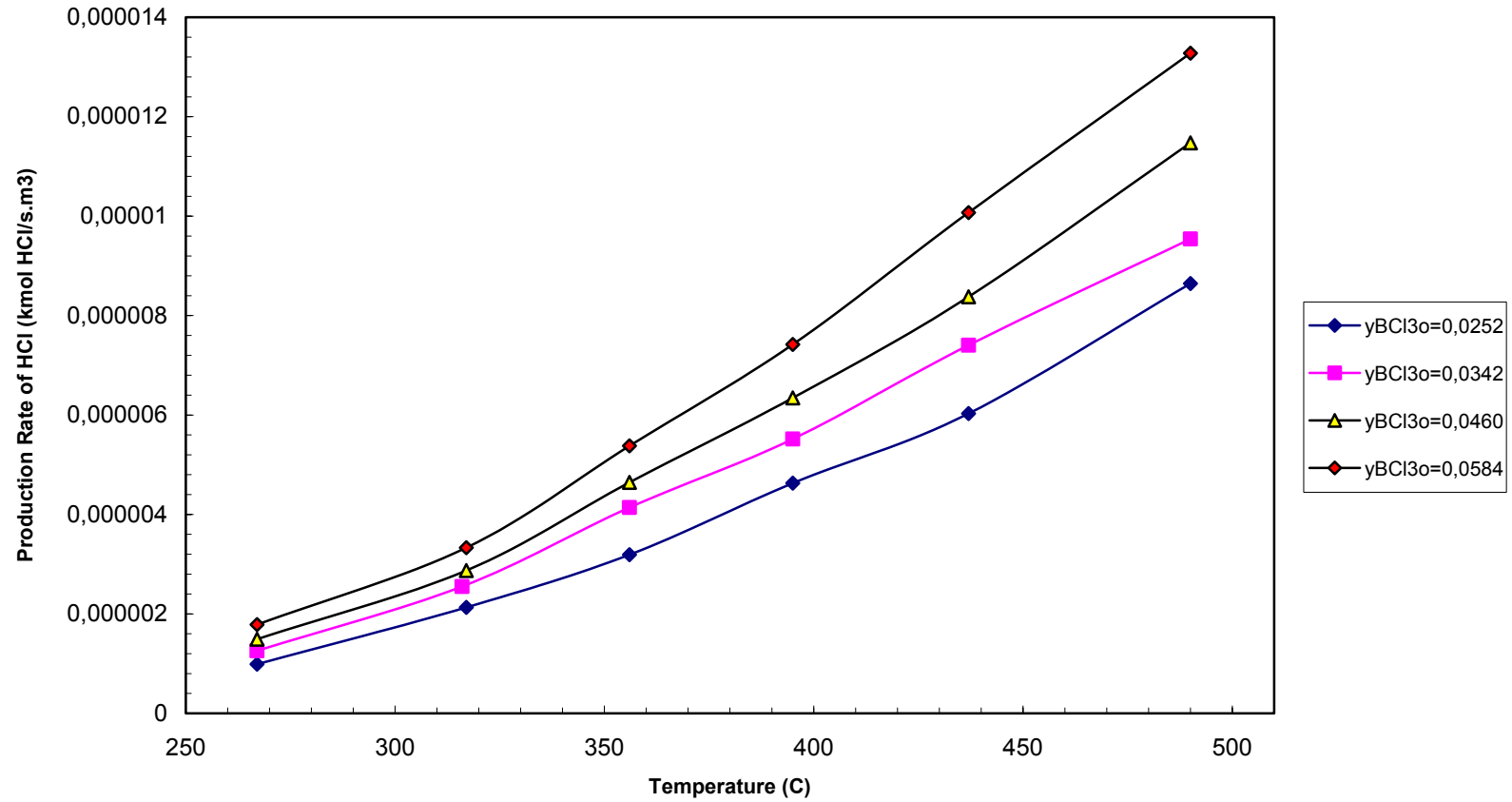


Figure 3.10 Effect of Temperature on Reaction Rate of HCl for Different Inlet Compositions of BCl₃

3.6 Results for BCl₃-H₂-He Experiments

In this set of experiments, the initial mole fraction of H₂ was changed, between 0.086 and 0.228. However, the mole fraction of BCl₃ was kept constant at 0.066. This is necessary to investigate the affect of H₂ in the reaction rate. Experiments were carried out at six different mole fractions of H₂ and different reactor temperatures.

Here helium was used to keep the volumetric flow rate of gas mixture constant. The volumetric flow rate of gas mixture was 200×10^{-6} m³/min in each experiment. Change of conversion with the inlet mole fraction of H₂ is given in Figure 3.11.

As expected, conversion has an ascending tendency with the increase in inlet mole fraction of H₂ and the reactor temperature (Figure 3.11 and Figure 3.12). The increase in the conversion with an increase in the reactor temperature is due to an increase in rate constant. There is an exponential relationship between temperature and reaction rate constant, k . Also, the ascending in conversion with an increase in inlet mole fraction of H₂ is reasonable because reaction rate is directly proportional with the outlet concentration of H₂. When the inlet mole fraction of H₂ is increased, the outlet concentration of H₂ is incidentally increased. In Figure 3.13, the reactor exit mole fraction of BHCl₂ as a function of reactor temperature is shown. As it is seen from the figure, the mole fraction of BHCl₂ has a descending tendency with the increase of reactor temperature above 500°C like in Figure 3.8. These two figures (Fig. 3.8 and Fig. 3.13) are consistent with each other. Figure 3.14 shows the effect of reactor on reaction rate of HCl. It is observed that the reaction rate of HCl increases with an increase in both reactor temperature and initial mole fraction of H₂.

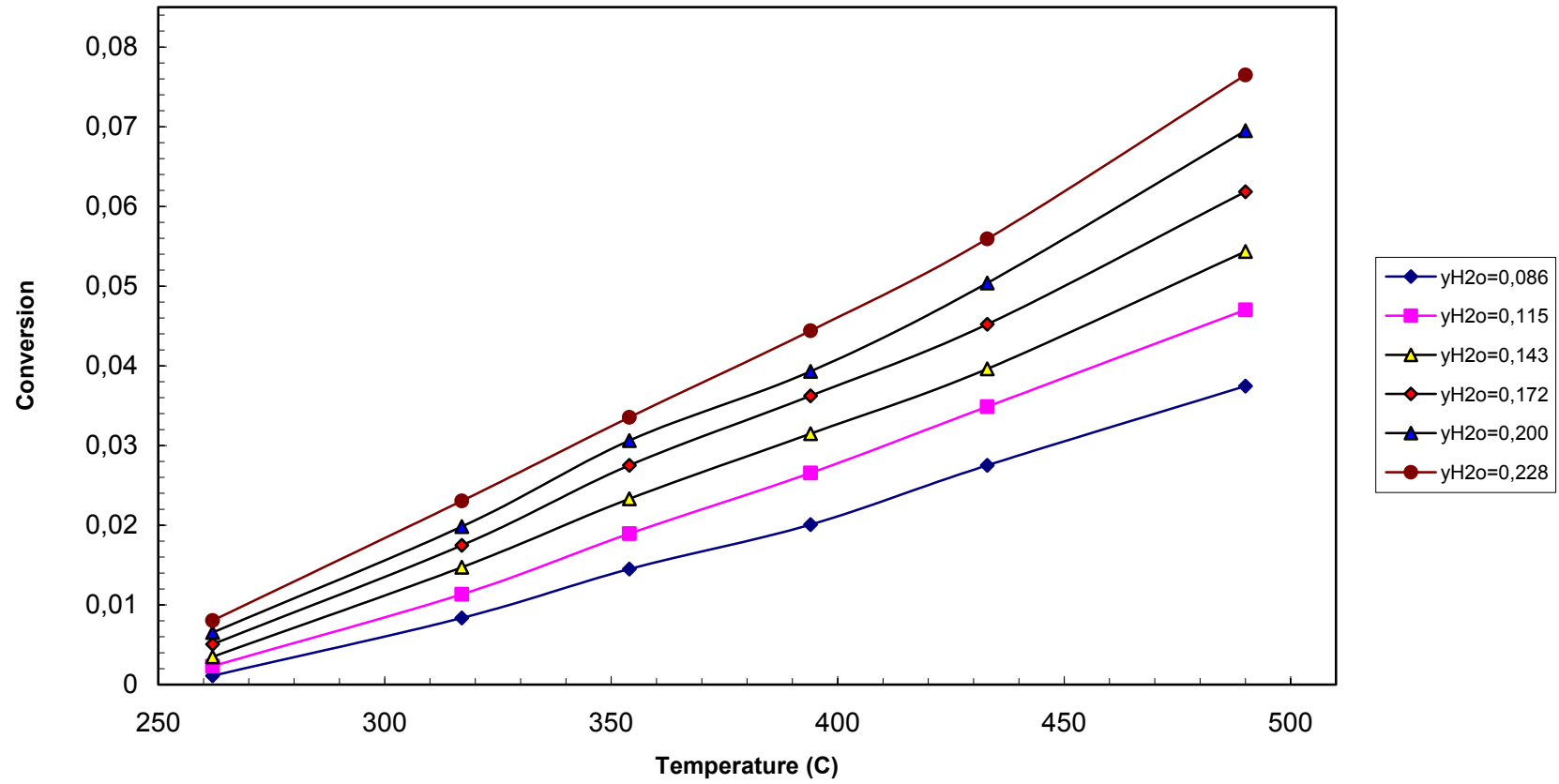


Figure 3.11 Change of Conversion with Different Inlet Compositions of H₂ at Various Reactor Temperatures

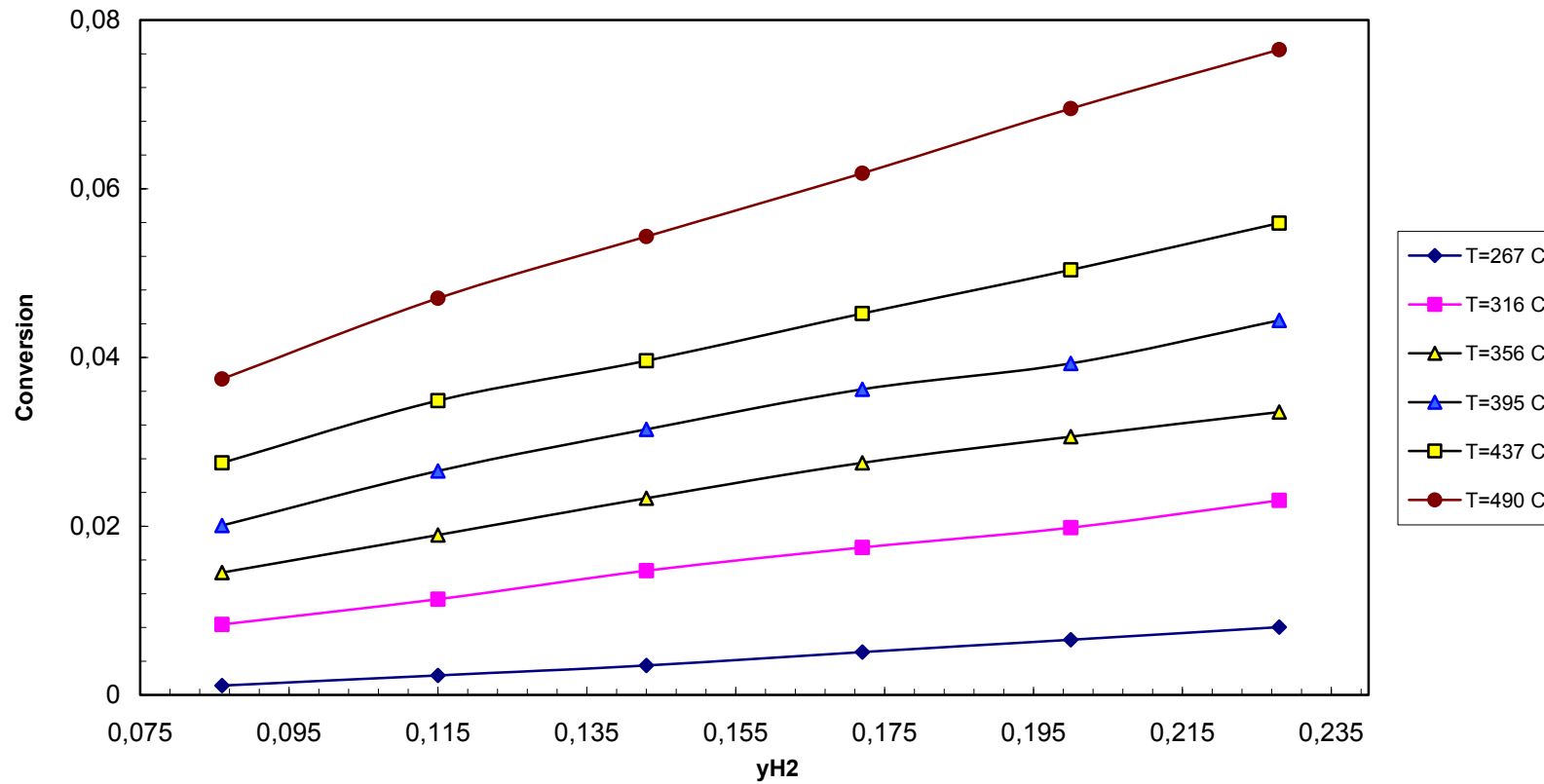


Figure 3.12 Effect of Inlet Mole Fraction of H₂ on Conversion for Different Reactor Temperatures

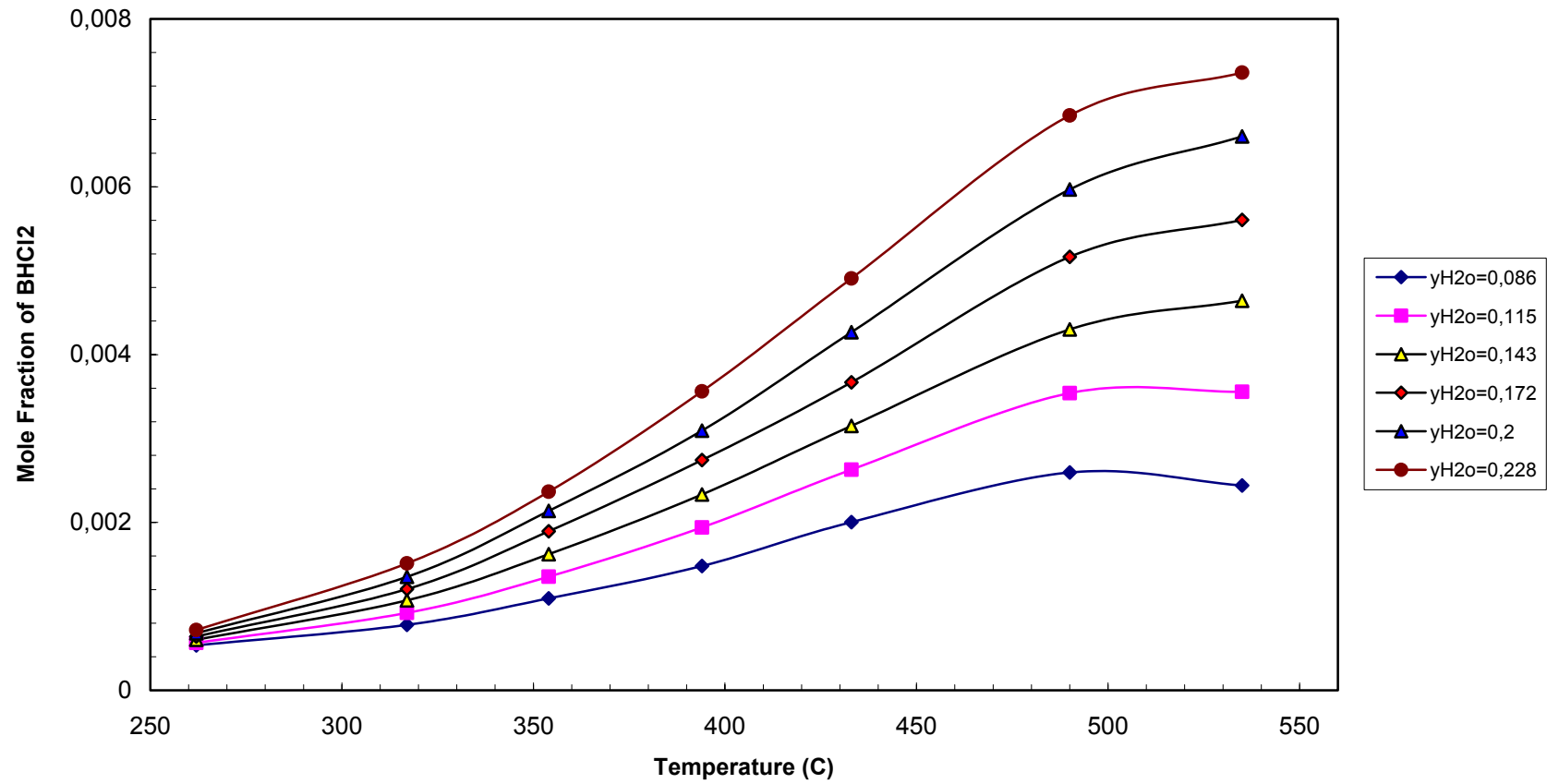


Figure 3.13 Effect of Temperature on the Mole Fraction of BHCl_2 for Different Inlet Compositions of H_2

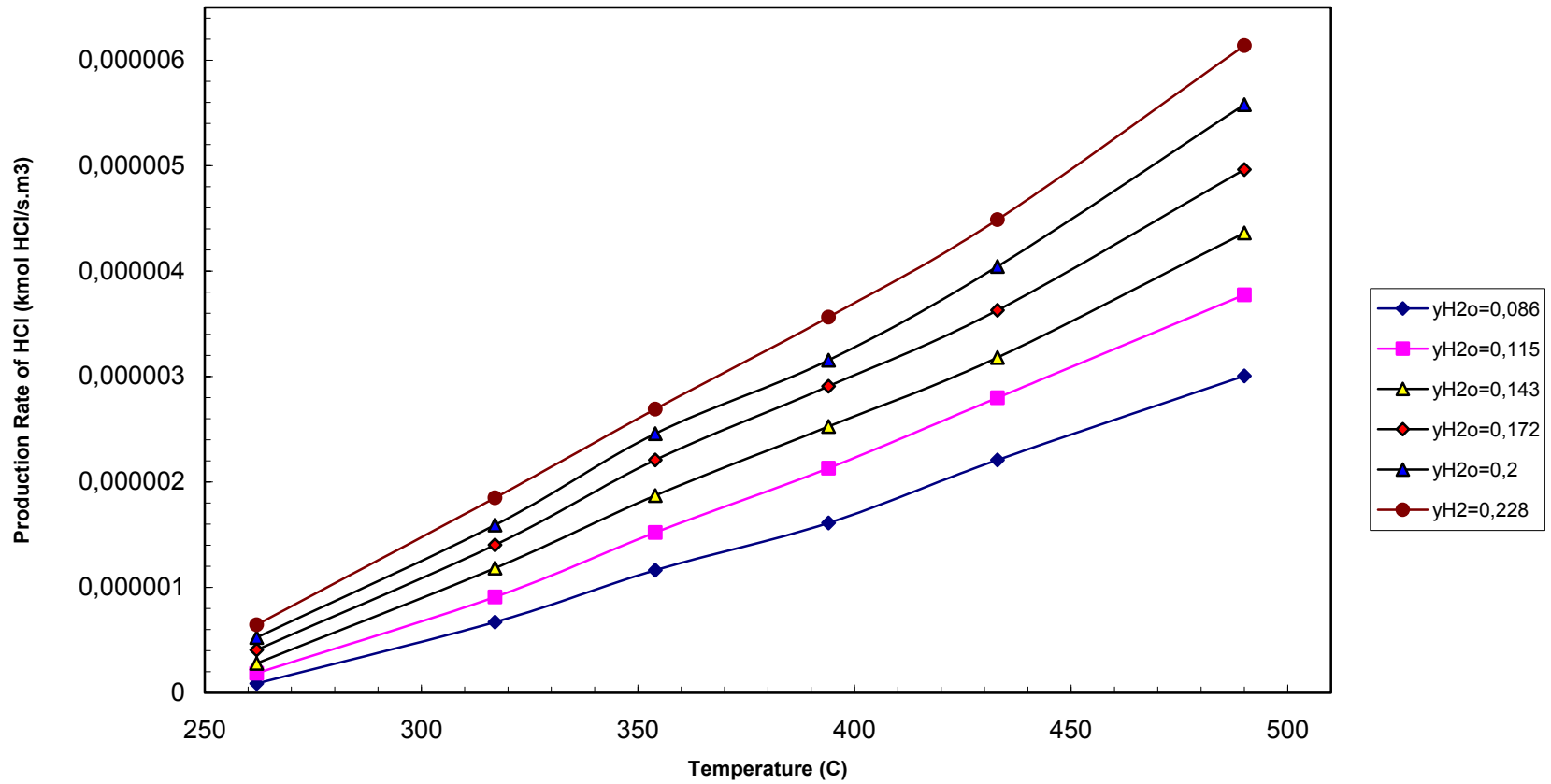


Figure 3.14 Change of Reaction Rate of HCl as a Function of Reactor Temperature for Different Inlet Compositions of H₂

3.7 Evaluation of Rate Parameters of the Proposed Rate Expression

As it is mentioned before, the experiments are divided into two sets named $\text{BCl}_3\text{-H}_2$ and $\text{BCl}_3\text{-H}_2\text{-He}$. The detailed information about these experimental groups is given in the experimental part. These two sets of experiments data were evaluated together to determine the rate parameters of rate expression.

Computer aided analysis was done in the evaluation of the data. The Arrhenius equation (Eqn. 3.15) was substituted into the reaction rate expression (Eqn. 3.14). The rate expression was obtained as;

$$R_{\text{BCl}_3} = -21.1204 \cdot \exp\left(-\frac{30.156}{R \cdot T}\right) \cdot (C_{\text{BCl}_3})^{0.54} \cdot (C_{\text{H}_2})^{0.64} \quad (3.17)$$

The proposed rate expression was tested with the experimental value of BCl_3 . Hooke and Jeeves iteration method was selected for the analysis of the data. Sixty data points were used in the iteration. The predicted value of reaction rate as a function of the experimental reaction rate is given in Figure 3.15. The variance of the model with the experimental results is 0.9926 and the correlation coefficient, R is 0.9963. The residual values of predicted reaction rate from the experimental results are shown in Figure 3.16. This amount of error is reasonable because of the $\text{BCl}_3\text{-H}_2$ experiments; the mole fraction of BCl_3 was adjusted by using FTIR peaks. This type of adjustment brings some error in the data analysis.

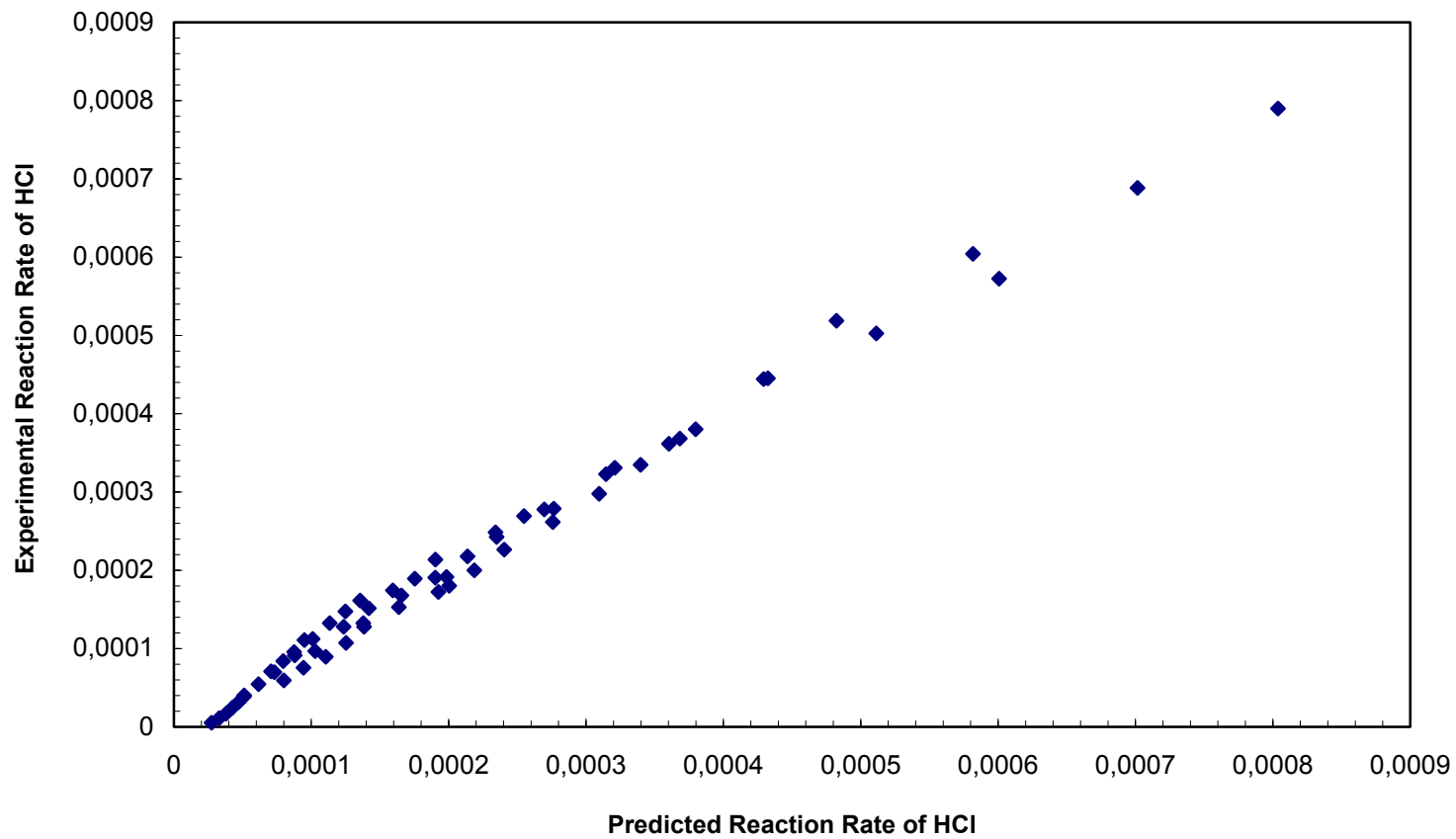


Figure 3.15 Graph for the Predicted and the Experimental Reaction Rate of HCl

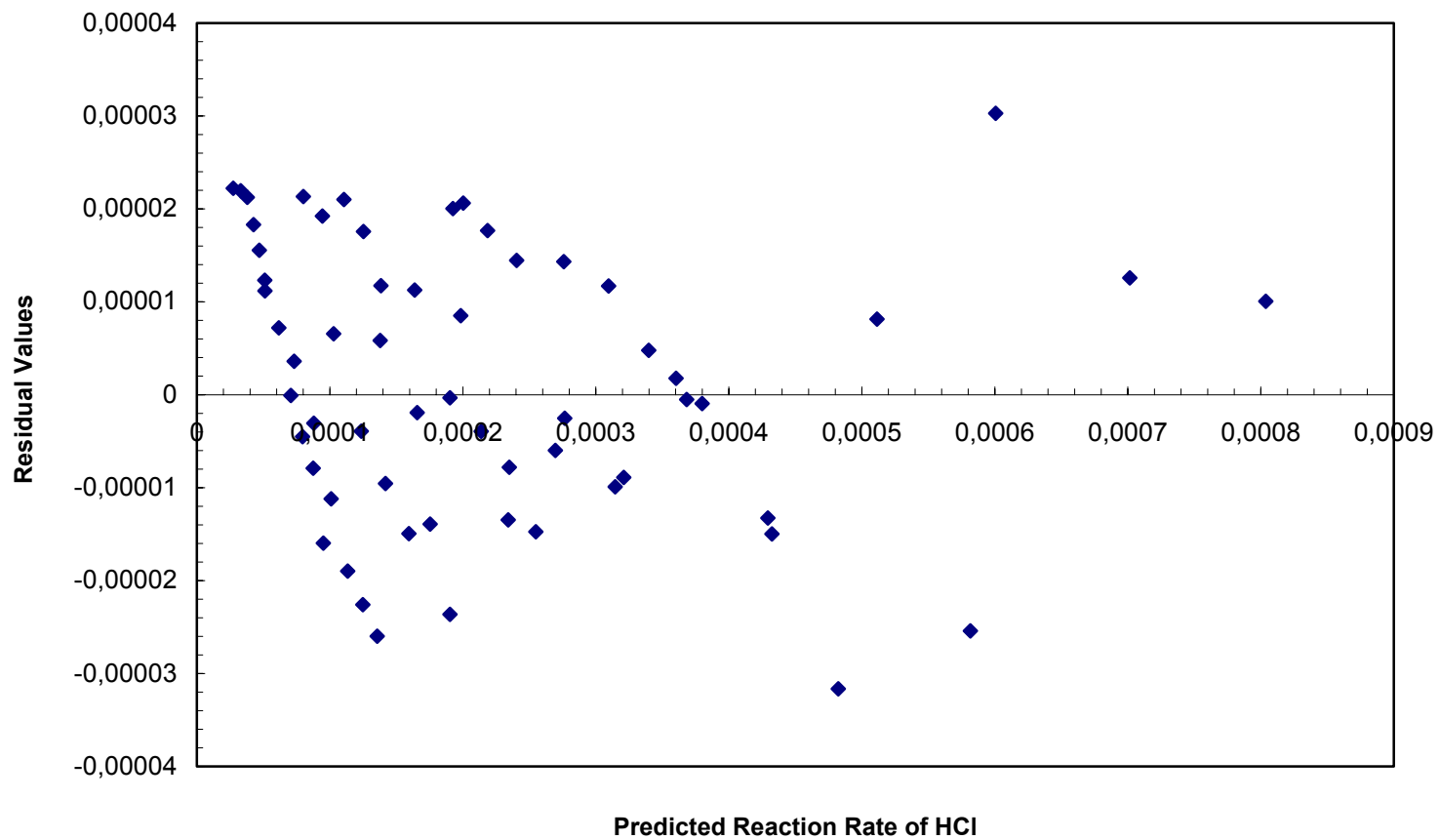


Figure 3.16 Predicted Reaction Rate of HCl versus Residual Values of Model Equation

CHAPTER 4

CONCLUSION

- It was observed that the gas phase reaction started above a reactor temperature of 170°C. Also, surface reaction took place over temperature of 500°C. The dichloroborane formation had a descending reaction rate over this temperature. This was due to the surface reaction
- It was observed that there was only one reaction taking place in the gas phase below a temperature of 500°C. Only BCl₃, HCl and BHCl₂ were observed in the FTIR spectra. No other chemical species were detected.
- The rate parameters of reaction rate were determined. The power of BCl₃ and H₂ concentrations in the rate expression were found to be 0.54 and 0.64, respectively. These orders are not digits, which imply that the chemical reaction is not a simple reaction with a complex mechanism. There are some side reactions in the gas phase of boron fiber production.
- The activation energy and frequency factor were found to be 30.156 *kJ/mol*

and $21.1204 \frac{(m^3)^{0.18}}{s \cdot (kmol)^{0.18}}$, respectively.

REFERENCES

Allendorf M. D., and **Melius C. F.**, “Understanding gas phase reactions in the thermal CVD of hard coatings using computational methods”, *Surface and Coating Technology*, Volume 108-109, 1998, Pages 191-199.

Ahıncı Ü., *Director General of Emet Etibor Corporation; Published in Anatolia Agency, 14 June 2003.*

Bhardwaj J. and **Krawitz A. D.**, “The structure of boron in boron fibres”, *J. Material Science*, Volume 18, 1983, Pages 2639-2649.

Buck M., and **Suplinskas R. J.**, “Continuous Boron Fiber MMCs”, *Eng. Materials Handbook Composites, Volume 1*, 1987, Pages 851-857.

Carlton H. E., **Oxley J. H.**, **Hall K. M.** and **Blacher J. M.**, “CVD second international conference”, **Blacher J. M.** and **Withers J. C.** ed., *The Electrochemical Society Softbound Symposium Series, New York, 1970, Page 209.*

Chiang M., “Boron in soils and plants”, *International Symposium on boron in soils and plants, September 1997, Page 274.*

Dilek S. N., Özbelge H. Ö., and Doğu T., “Kinetic studies for boron carbide formation in a dual impinging jet reactor”, *Ind. Eng. Chem. Res.*, Volume 40, 2001, Pages 751-755.

Ersoy, A., *Production of Boron Fiber by Chemical Vapor Deposition*, M.S. Thesis, METU-Ankara/Turkey, 1997, Pages 1-3.

Fogler H. S., *Elements of Chemical Reaction Engineering*, 2. ed., Prentice-Hall International Inc. Canada, 1992, Page 712

Gruber P. E., “CVD second international conference”, Blacher J. M. and Withers J. C. ed., *The Electrochemical Society Softbound Symposium Series*, New York, Volume 25, 1970, Pages 25-36.

Hauptfear E. A. and **Schmidt** L. D., “Kinetics of boron deposition from $\text{BBR}_3 + \text{H}_2$ ”, *Chemical Engineering Science*, Volume 49, Issue 15, August 1994, Pages 2467-2481.

Imaishi N., Sato T., Kimura M., and Akimaya Y., “Micro/Macro modeling of CVD synthesis”, *J. Crystal Growth*, Volume 180, 1997, Pages 680-690.

Jenkinson L. P., and Pollard R., “Thermal diffusion effects in chemical vapor deposition reactors”, *J. Electrochemistry Society*, *Solid-State Science and Technology*, Volume 124, 1977, Pages 1931-1937.

Jansson U., Olsson M., Stridh B., Carlsson J. O., Söderberg S., “Mechanical and tribological properties of chemically vapor-deposited boron carbide coatings”, *Materials Science and Engineering, Volumes 105-106, Part 2, December 1988, Pages 453-46.*

Kirk-Othmer, *Encyclopoeia of Chemical Technology, Volume 24, 4 ed., John Wiley&Sons Corporation, New York, Page 575.*

Kirk-Othmer, *Encyclopoeia of Chemical Technology, Volume 23, 4 ed., John Wiley&Sons Corporation, New York, Pages 1040-1077.*

Kirk-Othmer, *Encyclopoeia of Chemical Technology, Volume 4, 4 ed., John Wiley&Sons Corporation, New York, Pages 360-369.*

Lawrence J. B., Richard H. K., *Modern Composite Materials, Addison-Wesley Publishing Company; 1967.*

Maham J. E., *Physical Vapor Deposition of Thin Films, John Wiley&Sons, Published in 2000, Pages 1-19.*

Michaelidis M., and Pollard J., “Analysis of chemical vapor deposition of boron”, *J. Electrochemistry Society, Solid-State Science and Technology, Volume 131, 1984, Pages 860-867.*

Park J. H., *Chemical Vapor Deposition, Volume 2, ASM International, 1. Ed., July 2001, Pages 1-23.*

Sekine T., Nakanishi N., and Kato E., “Kinetics of chemical vapor deposition of boron thin film on tungsten substrate”, *J. Japan Inst. Metals, Volume 53, 1989, Pages 698-703.*

Sezgi N. A., Ersoy A., Doğu T. and Özbelge H. Ö., “CVD of boron and dichloroborane formation in a hot-wire fiber growth reactor”, *Chemical Engineering and Processing, Volume 40, Issue 6, November 2000, Pages 525-530.*

Sezgi N. A., Doğu T. and Özbelge H. Ö., “Mechanism of CVD of boron by hydrogen reduction of BCl_3 in a dual impinging-jet reactor”, *Chemical Engineering Science, Volume 54, Issues 15-16, July 1999, Pages 3297-3304.*

Sezgi N. A., Doğu T. and Özbelge H. Ö., “ BHCl_2 formation during chemical vapor deposition of boron in a dual impinging jet reactor”, *Ind. Eng. Chem. Res., Volume 36, 1997, Pages 5537-5540.*

Sezgi N. A., *Boron Fiber Production, Ph.D Thesis, METU-Ankara/Turkey, 1996, Pages 1-15.*

Talley C. P., Clark W. J., Wawner F. E., Jr., J. E. Schultz, and K. M. Gunn, “Boron reinforcements for structural composites,” *Air force Technical Documentary Report Number ASD-TDR-63-396, April 1963, Page 434.*

Vandelbulke L. G., “CVD of boron from impinging jets”, *J. Electrochemistry Society, Solid-State Science and Technology, Volume 124, 1977, Pages 1931-1937.*

Vandelbulke L. G. and **Vuillard** G., “Structure of deposits-process relationships in the CVD of boron”, *J. Electrochemistry Society, Solid-State Science and Technology, Volume 124, 1977, Pages 1938-1942.*

Vinson J. R., and **Chou** Tsu-Wei, *Composite Materials and Their Use in Structures* John Wiley & Sons, 1975.

Yalaz N., Gözmen T., Kocakuşak S., and Kalafatoğlu E., *İnorganik Bor Bileşikleri Kaynak Araştırması Bor Elyafı ve Filmleri, TÜBİTAK, Gebze-Kocaeli, 1987.*

APPENDIX A

CALIBRATION METHODS

To perform the chemical analysis of outlet gas mixture, it is necessary to evaluate the relationship between the concentrations of gases involved and the peak heights of the peak areas obtained from the FT-IR spectra. The calibration curves were drawn using the gas concentration and the peak area values for each gas. Calibration methods for each gas are explained in detail.

A.1 Calibration Method for BCl_3 Concentration Measurement

The calibration method for BCl_3 gas is based on the weight change of U-tube. The boron trichloride in the outlet gas mixture was collected in the U-tube for a period of time. During the calibration experiments, gaseous BCl_3 was condensed in a U-tube which was submerged into thermos containing liquid nitrogen. The thermos was closed with a stopper to prevent the evaporation of nitrogen in it. Boron trichloride is in gaseous form at pressure of 1 atm and a temperature of 15°C . A U-tube was added to the original experimental set-up. U-tube was made of pyrex and

filled with broken glass pieces to increase the contact surface. Boron trichloride was captured in the U-tube. The experimental set-up is given in Figure A.1

Before starting the experiment, the U-tube with broken glass pieces were weighed and recorded. Then, the volumetric flow rates of BCl₃ and H₂ were adjusted. Total volumetric flow rate was set to 200x10⁻⁶ m³/min. The gas mixture was passed into the gas cell of FTIR. The temperature of the gas cell was kept constant at 110°C. The chemical analysis of the gas mixture was carried out until the peak area of the BCl₃ obtained in the FT-IR spectra remained at a constant value. After the peak area of BCl₃ remained constant, BCl₃ was condensed in the U-tube. Two glass valves were connected to the inlet and outlet streams of the U-tube. Three directional valve at the inlet stream was used not to allow the gas mixture to pass through the U-tube during the flow rate adjustments. The other one was used to prevent escape of the BCl₃ gas during the process of taking the U-tube out from the liquid nitrogen. During the calibration experiment, the H₂ was discarded to the atmosphere but BCl₃ was condensed and separated from the outlet gas mixture. At the end of the experiment, the U-tube was reweighed and recorded. The weight difference between the initial and final weight of U-tube gave the weight of BCl₃ condensed in the U-tube. Finally, the ideal gas law was used to determine the mole fractions of BCl₃. This procedure was repeated for different mol fraction of BCl₃. Sample calculation is given below;

Sample Calculation:

$$W_{BCl_3} = W_{U-tube|_{t=t}} - W_{U-tube|_{t=0}} \quad (\text{A.1})$$

$$P \cdot \dot{V}_{mix} \cdot t \cdot y_{BCl_3} = n_{BCl_3} \cdot R \cdot T \quad (\text{A.2})$$

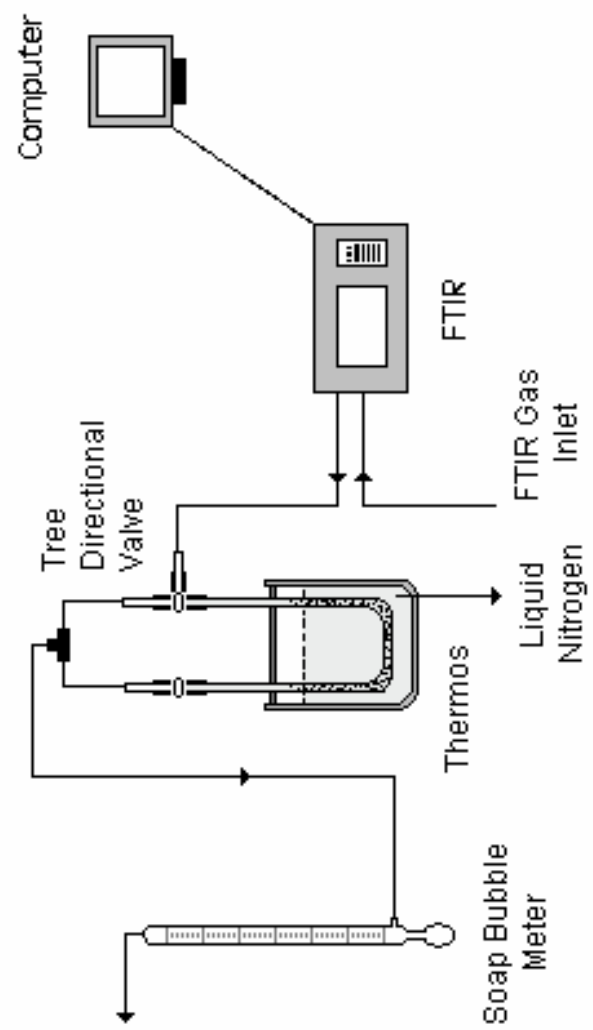


Figure A.1. Calibration Set-up for Boron Trichloride

At normal conditions (1 atm, 298.15 K), 1 mol of gas has 22400 cm³ volume. The temperature and the pressure of the gas mixture are assumed to be 298.15 K and 1 atm, respectively. Equation A.5 is obtained by substituting equation A.3 into equation A.4;

$$1\text{atm} \cdot 22.4\text{lt} = 1\text{mol} \cdot 0.08206 \frac{\text{atm} \cdot \text{lt}}{\text{mol} \cdot \text{K}} \cdot 298.15\text{K} \quad (\text{A.3})$$

$$P \cdot \dot{V}_{\text{mix}} \cdot t \cdot y_{\text{BCl}_3} = \frac{W_{\text{BCl}_3}}{M_{\text{BCl}_3}} \cdot R \cdot T \quad (\text{A.4})$$

$$y_{\text{BCl}_3} = \frac{W_{\text{BCl}_3} \cdot 22400}{M_{\text{BCl}_3} \cdot \dot{V}_{\text{mix}} \cdot t} \quad (\text{A.5})$$

$$t = (\text{min}) \quad W_{\text{BCl}_3} = (\text{gram}) \quad \dot{V}_{\text{mix}} = (\text{cm}^3/\text{min})$$

The equation (A.6) gives the relationship between mol fraction of boron trichloride and area of the peak at a given wavenumber.

$$y_{\text{BCl}_3} = \frac{(0.5097 \cdot 10^{-3} + 0.454 \cdot 10^{-6} \cdot \text{Area})}{(1 - 0.5977 \cdot 10^{-2} \cdot \text{Area} + 0.9023 \cdot 10^{-5} \cdot \text{Area}^2)} \quad (\text{A.6})$$

Calibration curve for BCl₃ is given in Figure A.2.

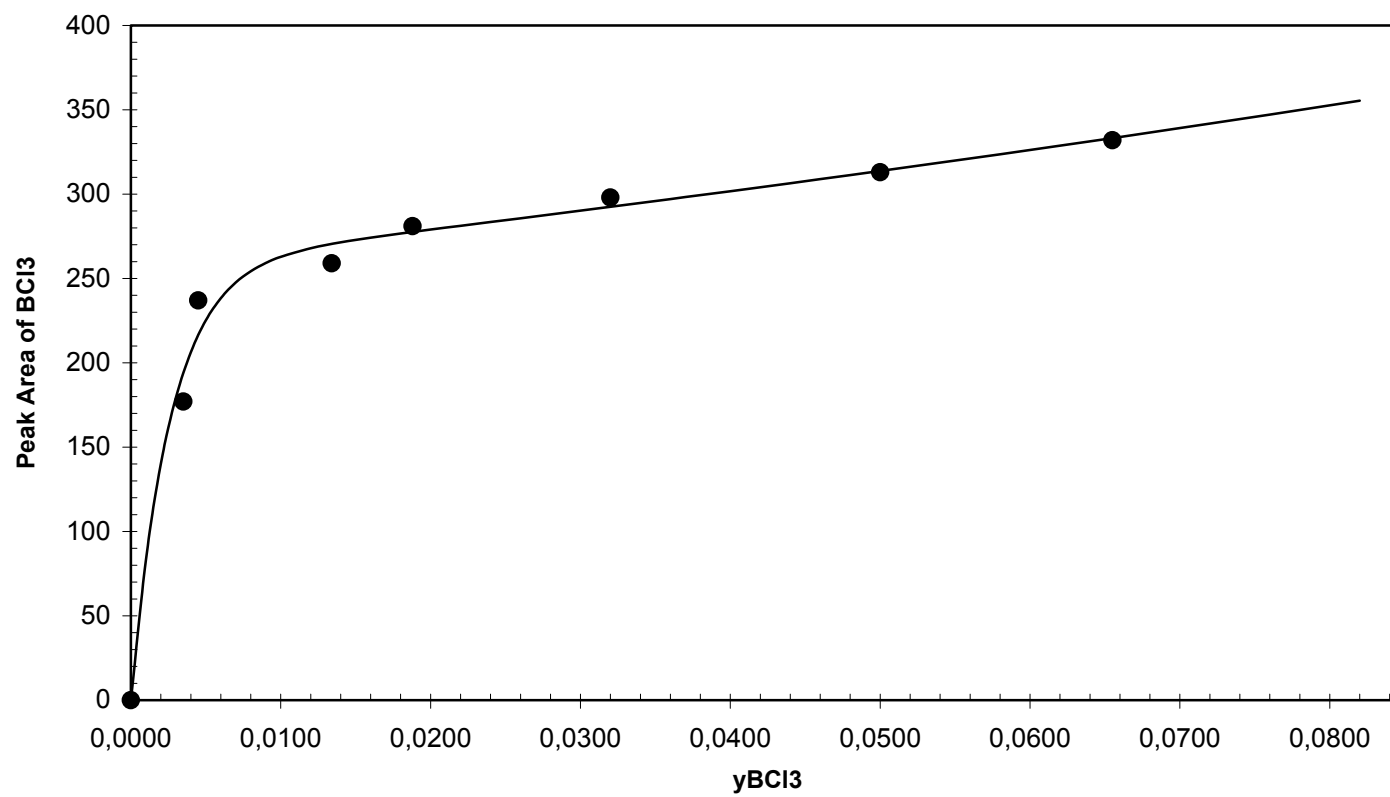


Figure A.2. Calibration Curve for Boron Trichloride at a Wavenumber Range of 1100-850 cm^{-1}

A.2 Calibration Method for Hydrochloric Acid Concentration Measurement

The actual experimental set-up was used for the calibration of hydrochloric acid, but the HCl gas tube was replaced with one of the reactant tubes since HCl is a very corrosive chemical, rotameter was used to adjust its volumetric flow rate. In the experiments, helium was used as a carrier gas. The volumetric flow rate of helium was adjusted by using mass flow controller. Then, the total volumetric flow rate of gas mixture was set to $200 \times 10^{-6} \text{ m}^3/\text{min}$. The temperature of the gas cell was kept constant at 110°C . The apparent flow rate of the gas mixture was checked using a soap bubble meter. A group of peaks for the HCl gas were observed in the spectrum at a wavenumber range of 2500 and 3100 cm^{-1} . The FTIR spectra were taken until the peak area of HCl remained at a constant value. The same procedure was applied for the different concentrations of the HCl gas. The peak height of HCl corresponding to each concentration was plotted in Figure A.3. The relation between mol fraction of HCl and the peak height is formulated below as;

$$y_{\text{HCl}} = -1.1275 \cdot (H_{\text{HCl}})^3 + 0.8222 \cdot (H_{\text{HCl}})^2 + 0.04362 \cdot H_{\text{HCl}} - 0.3113 \cdot 10^{-3} \quad (\text{A.7})$$

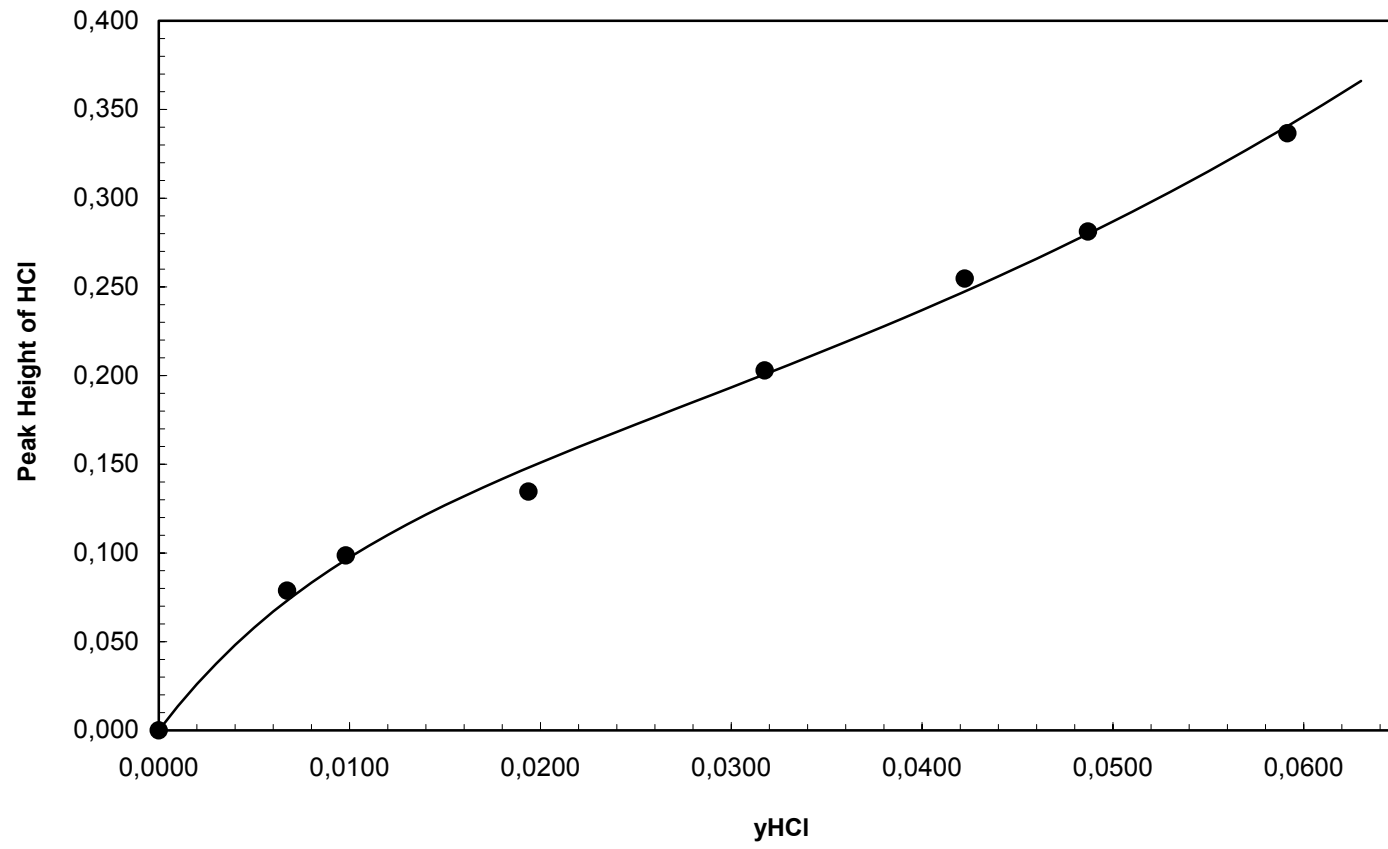


Figure A.3. Calibration Curve for Hydrochloric Acid at a Wavenumber of 2798 cm⁻¹

APPENDIX B

CALCULATIONS FOR DOUBLE PIPE HEAT EXCHANGER

The heat exchanger, which is used to cool the outlet gas mixture, is constructed from stainless steel. The dimensions of the heat exchanger are given in the experimental part. Here, the calculation performed for this heat exchanger is given in details. The aim of this calculation is to find out the outlet temperature of the gas mixture. As it is mentioned before, it is necessary to cool the gas mixture as soon as possible to cease the gas phase reaction.

The type of the heat exchanger is double pipe. The inner pipe of heat exchanger, which outlet gas mixture is passed through, is filled with packing materials to increase the contact surface area of the gas. Also, packing materials reduces the volume of the inner pipe. Volume between the reactor and the FT-IR is very important because the pipe line between the reactor and the FT-IR behaves as a PFR. Tap water is used as a coolant. The cooling water is passed through outer pipe. Ceramic saddle ring is used as packing. The data for the physical properties and dimensions of the packing were taken from Perry's Chemical Engineering Handbook.

The calculations performed here are only for helium. In the calculations, h denotes hot fluid (helium), c denotes cold fluid (water) and p denotes packed bed. The physical properties of helium, water and packing materials are calculated at average temperatures. It is assumed that the outlet temperature of the helium is close to the inlet temperature of the water. This assumption is acceptable because the mass flow rate of gas mixture is negligible when it is compared with the mass flow rate of water. The physical properties of helium at average temperature are given as;

$$\begin{array}{ll}
 Ta_h = 450K & \rho_h = 0.7485 \frac{kg}{m^3} \\
 Tin_h = 723K & k_h = 35.8 \cdot 10^{-3} \frac{watt}{m \cdot K} \\
 V_h = 200 \frac{cm^3}{min} & \mu_h = 239.6 \cdot 10^{-7} \frac{kg}{m \cdot s} \\
 Cp_h = 1050 \frac{J}{kg \cdot K} & Npr_h = 0.703
 \end{array}$$

The physical properties of helium are used to determine the heat transfer coefficient of inner pipe. The physical properties of H₂O (cold fluid) at average temperature are given as;

$$\begin{array}{ll}
 Ta_c = 285K & \rho_c = 1000 \frac{kg}{m^3} \\
 Tin_c = 283K & k_c = 590 \cdot 10^{-3} \frac{watt}{m \cdot K} \\
 m_c = 2 \frac{kg}{min} & \mu_c = 1225 \cdot 10^{-6} \frac{kg}{m \cdot s}
 \end{array}$$

$$Cp_c = 4179 \frac{J}{kg \cdot K}$$

$$Npr_c = 8.81$$

The dimensions of the heat exchanger;

$$D_i = 1.8 \cdot 10^{-2} m$$

$$D_o = 2.0 \cdot 10^{-2} m$$

$$D_i' = 3.65 \cdot 10^{-2} m$$

$$D_o' = 4.0 \cdot 10^{-2} m$$

$$L = 27 \cdot 10^{-2} m$$

$$T_w = 283K$$

Dimensions and physical properties of ceramic saddle rings;

$$D_p = 6 \cdot 10^{-3} m$$

$$\rho_p = 864 \frac{kg}{m^3}$$

$$a = 984 \frac{m^2}{m^3}$$

$$f_p = 302 \frac{1}{m}$$

$$\varepsilon_o = 0.65$$

Now, it is possible to calculate the convective heat transfer coefficients for both water and for helium. As it is seen from the given data that there are two unknowns (T_{cout} and T_{hout}), so that two equations are necessary to solve this problem. This problem has a trial and error solution. There is only one way to manage the hardness of trial and error solution. This is the NTU (Number of Transfer Unit) method. It facilitates the calculations. Without this method, it is necessary to use trial and error method. That is why, NTU method is used. Calculation done for the inside heat transfer coefficient (h_{in}) for helium case is given below;

$$A_h = \frac{\pi \cdot D_i^2}{4} \quad (\text{B.1})$$

$$A_h' = \pi \cdot D_i \cdot L \quad (\text{B.2})$$

$$V_h = 3.333 \cdot 10^{-6} \frac{m^3}{s}$$

$$m_h = \rho_h \cdot V_h \quad (\text{B.3})$$

$$m_h = 2.495 \cdot 10^{-6} \frac{kg}{s}$$

$$v_h = \frac{V_h}{A_h} \quad (\text{B.4})$$

$$v_h = 0.013 \frac{m}{s}$$

$$G = v_h \cdot \rho_h \quad (\text{B.5})$$

$$G = 9.805 \cdot 10^{-3} \frac{kg}{m^2 \cdot s}$$

$$Nre_h = \frac{G \cdot D_p}{\mu_h} \quad (\text{B.6})$$

$$Nre_h = 2.455$$

Packed-Bed operations occur, when the fluid velocity is low or the particle size large so that fluidization does not occur. For such operations, the formula of Leva [Ind. Che. Eng., 42, 2498, (1950)] is acceptable;

$$h_i = 0.813 \cdot \frac{k_h}{D_i} \cdot \exp\left(-6 \frac{D_p}{D_i}\right) \cdot \left(\frac{D_p \cdot G}{\mu_h}\right)^{0.9} \quad \text{for } \frac{D_p}{D_i} \leq 0.35 \quad (\text{B.7})$$

$$h_i = 0.491 \frac{kg}{s^3 \cdot K}$$

$$\mu_{w_h} = 178.2 \cdot 10^{-7} \frac{kg}{m \cdot s}$$

$$A_c = \pi \cdot \frac{[(D_i')^2 - D_i^2]}{4} \quad (\text{B.8})$$

$$A_c = 7.322 \cdot 10^{-4} m^2$$

$$A_c' = \pi \cdot D_o \cdot L \quad (\text{B.9})$$

$$A_c' = 0.017 m^2$$

$$V_c = 3.333 \cdot 10^{-5} \frac{m^3}{s}$$

$$v_c = \frac{V_c}{A_c} \quad (\text{B.10})$$

$$v_c = 0.046 \frac{m}{s}$$

$$Nre_c = \frac{D_i' \cdot v_c \cdot \rho_h}{\mu_c} \quad (\text{B.11})$$

$$Nre_c = 1.356 \cdot 10^3$$

Nre_c is lower than 2100, so that flow is laminar. For laminar flow, the equation B.12 is acceptable for water. The wall temperature of the inner pipe is assumed to be equal to inlet temperature of water. Hence, $\mu_{w_h} = \mu_c$ is valid;

$$\frac{h_o \cdot D_i'}{k_c} = 1.86 \cdot \left(Nre_c \cdot Npr_c \cdot \frac{D_i'}{L} \right)^{\frac{1}{3}} \cdot \left(\frac{\mu_c}{\mu_{w_c}} \right)^{0.14} \quad (\text{B.12})$$

$$h_o = 352.786 \frac{kg}{s^3 \cdot K}$$

The thickness of pipe is equal to;

$$\Delta x = \frac{(D_o - D_i)}{2} \quad \text{(B.13)}$$

$$\Delta x = 10^{-3} m$$

The thermal conductivity of copper is equal to;

$$k_{cu} = 377 \frac{\text{watt}}{\text{m} \cdot \text{K}} \text{ at } 100^\circ \text{C}$$

It is not changing with the change of temperature.

$$U = \frac{1}{\left[\frac{1}{h_i} + \frac{\Delta x}{k_{cu}} \cdot \frac{A_h'}{(A_c' - A_h')} + \frac{1}{h_o} \cdot \left(\frac{A_h'}{A_c'} \right) \right]} \quad \text{(B.14)}$$

$$U = 0.491 \frac{\text{kg}}{\text{s}^3 \cdot \text{K}}$$

From now on, NTU Method is used to solve the remaining part of problem.

At first, it is necessary to find out C_{\min} and C_{\max} ;

$$C_c = m_c \cdot Cp_c \quad \text{(B.15)}$$

$$C_c = 139.3 \frac{\text{kg}}{\text{s}^3 \cdot \text{K}}$$

$$C_h = m_h \cdot Cp_h \quad \text{(B.16)}$$

$$C_h = 2.62 \cdot 10^{-3} \frac{kg}{s^3 \cdot K}$$

$$C_{\max} = C_c \quad \text{and} \quad C_{\min} = C_h$$

$$C = \frac{C_{\min}}{C_{\max}} \tag{B.17}$$

$$C = 1.881 \cdot 10^{-5}$$

$$NTU = \frac{U \cdot Aht_h}{C_{\min}} \tag{B.18}$$

$$NTU = 2.859$$

The effectiveness factor for the counter current flow is given as;

$$\varepsilon = \frac{1 - \exp[-(1 - C) \cdot NTU]}{1 - C \cdot \exp[-(1 - C) \cdot NTU]} \tag{B.19}$$

$$\varepsilon = 0.943$$

From the following equations, it is possible to find out heat transfer rate;

$$Q = \varepsilon \cdot C_{\min} (Tin_h - Tout_c) \tag{B.20}$$

$$Tout_c = \frac{Q}{m_c \cdot Cp_c} + Tin_c \tag{B.21}$$

$$Tout_c = 283.008K$$

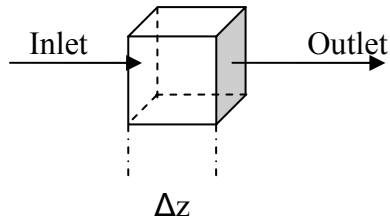
$$Q = m_h \cdot Cp_h \cdot (Tin_h - Tout_h) \tag{B.22}$$

$$Tout_h = Tin_h - \frac{Q}{m_h \cdot Cp_h}$$

$$Tout_h = 308.23K$$

B.1. Temperature Profile along the Length of the Heat Exchanger

The temperature profile of the gas mixture is important for us. It helps us to determine the length of the pipe to decrease the temperature of gas mixture to a reasonable value. It is assumed that the wall temperature doesn't change with the length. Also, there is no radial temperature change along the heat exchanger. There is only axial temperature gradient. The energy balance for the chosen system is given;



$$m_h \cdot C_{p_h} \cdot T|_z - m_h \cdot C_{p_h} \cdot T|_{z+\Delta z} - h_i \cdot a \cdot A_h \cdot (T - T_{a_c}) \cdot \Delta z = 0 \quad (\text{B.23})$$

A control volume is chosen and energy balance written for this control volume. Both sides of Eqn. B.23 are divided by Δz ; and the Eqn. B.24 is obtained;

$$m_h \cdot C_{p_h} \cdot dT = -h_i \cdot a \cdot A_h \cdot (T - T_{a_c}) \cdot dz \quad (\text{B.24})$$

The following equation (B.25) is obtained by integrating the Eqn. B.24;

$$\ln \left(\frac{T - T_w}{T_{in_h} - T_w} \right) = \left(\frac{h_i \cdot a \cdot A_h}{m_h \cdot C_{p_h}} \right) \cdot z \quad (\text{B.25})$$

Arranging the equation (B.25), the following equation is obtained;

$$T(z) = T_w + (Tin_h - T_w) \cdot \exp \left[- \left(\frac{h_i \cdot a \cdot A_h}{m_h \cdot Cp_h} \right) \cdot z \right] \quad (\text{B.26})$$

Temperature of the gas mixture is exponentially changing with the length of heat exchanger. The results of equation (B.26) are tabulated in Table B.1. Using the data in Table B.1, temperature profile along the length of the heat exchanger is plotted in Figure B.1.

Table B.1. Temperature Change of Helium with Length of Heat Exchanger

z (m)	T (K)	z (m)	T (K)	z (m)	T (K)	z (m)	T (K)
0	723.00	0.07	299.49	0.14	283.62	0.21	283.02
0.01	558.23	0.08	293.31	0.15	283.39	0.22	283.01
0.02	455.16	0.09	289.45	0.16	283.24	0.23	283.01
0.03	390.69	0.1	287.03	0.17	283.15	0.24	283.01
0.04	350.36	0.11	285.52	0.18	283.09	0.25	283.00
0.05	325.13	0.12	284.58	0.19	283.06	0.26	283.00
0.06	309.36	0.13	283.99	0.2	283.04	0.27	283.00

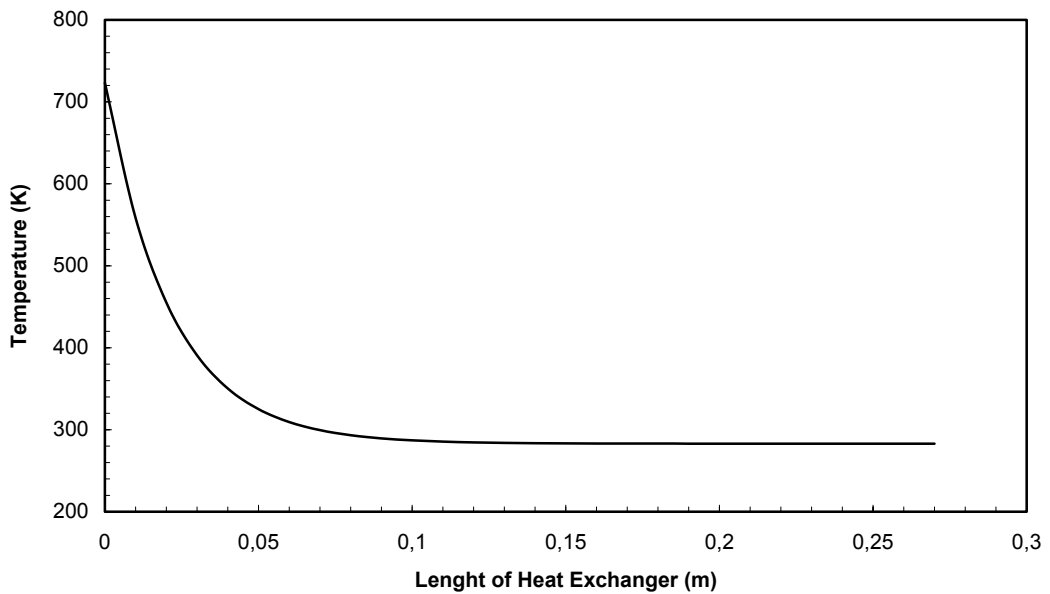


Figure B.1. The Temperature Profile of Helium in the Heat Exchanger

APPENDIX C

EXPERIMENTAL DATA

The raw data of the experiments are tabulated in Tables C.1-C.11.

Table C.1. The Raw Data for BCl₃-H₂ Experiments (Tot. Vol. Flowrate: 209.07 ml/min, y_{BCl_{3o}}=0.025 and y_{H_{2o}}=0.975)

Run Number	T _r (C)	t (min)	Y _{HClf}	Y _{BCl_{3f}}	Y _{BHCl_{2f}}	Y _{H_{2f}}
BCI3-1-65	267	35	0.00081	0.01957	0.00090	0.97399
BCI3-1-57	317	35	0.00175	0.01894	0.00170	0.97305
BCI3-1-49	356	40	0.00263	0.01827	0.00247	0.97218
BCI3-1-42	395	40	0.00381	0.02012	0.00373	0.97099
BCI3-1-33	437	30	0.00496	0.02126	0.00537	0.96984
BCI3-1-24	490	35	0.00711	0.01977	0.00688	0.96769
BCI3-1-16	538	35	0.00940	0.01932	0.00668	0.96540

Table C.2. The Raw Data for BCl₃-H₂ Experiments (Tot. Vol. Flowrate: 211.02 ml/min, y_{BCl_{3o}}=0.034 and y_{H_{2o}}=0.966)

Run Number	T _r (C)	t (min)	Y _{HClf}	Y _{BCl_{3f}}	Y _{BHCl_{2f}}	Y _{H_{2f}}
BCI3-2-64	267	35	0.00103	0.03265	0.00114	0.96477
BCI3-2-57	317	35	0.00210	0.02785	0.00206	0.96370
BCI3-2-49	356	40	0.00340	0.02328	0.00313	0.96240
BCI3-2-42	395	40	0.00454	0.02840	0.00460	0.96126
BCI3-2-33	437	30	0.00609	0.02891	0.00639	0.95971
BCI3-2-24	490	35	0.00785	0.02573	0.00768	0.95795
BCI3-2-16	538	30	0.01118	0.02622	0.00803	0.95462

Table C.3. The Raw Data for BCl₃-H₂ Experiments (Tot. Vol. Flowrate: 213.62 ml/min, y_{BCl_{3o}}=0.046 and y_{H_{2o}}=0.954)

Run Number	T _r (C)	t (min)	Y _{HClf}	Y _{BCl_{3f}}	Y _{BHCl_{2f}}	Y _{H_{2f}}
BCI3-3-64	267	35	0.00123	0.04180	0.00126	0.95277
BCI3-3-57	317	35	0.00236	0.04005	0.00227	0.95164
BCI3-3-49	356	40	0.00382	0.04323	0.00367	0.95018
BCI3-3-42	395	40	0.00522	0.04035	0.00546	0.94878
BCI3-3-33	437	30	0.00689	0.04502	0.00723	0.94711
BCI3-3-24	490	35	0.00944	0.03976	0.00906	0.94456
BCI3-3-16	538	30	0.01255	0.03991	0.00961	0.94145

Table C.4. The Raw Data for BCl₃-H₂ Experiments (Tot. Vol. Flowrate: 215.7 ml/min, y_{BCl₃0}=0.058 and y_{H₂0}=0.942)

Run Number	T _r (C)	t (min)	y _{HClf}	y _{BCl₃f}	y _{BHCl₂f}	y _{H₂f}
BCI3-4-64	267	35	0,00147	0,05685	0,00144	0,94015
BCI3-4-57	317	35	0,00274	0,05071	0,00262	0,93888
BCI3-4-49	356	40	0,00442	0,05404	0,00437	0,93720
BCI3-4-42	395	40	0,00610	0,04510	0,00657	0,93552
BCI3-4-33	437	30	0,00828	0,05622	0,00864	0,93334
BCI3-4-24	490	35	0,01092	0,04711	0,01029	0,93070
BCI3-4-16	538	30	0,01426	0,04823	0,01057	0,92736

Table C.5. The Raw Data for BCl₃-H₂-He Experiments (Tot. Vol. Flowrate: 207.18 ml/min, y_{BCl₃0}=0.066, y_{H₂0}=0.086 and y_{He}=0.848)

Run Number	T _r (C)	t (min)	y _{HClf}	y _{BCl₃f}	y _{BHCl₂f}	y _{H₂f}
H2-15-65	262	35	0.00007	0.06507	0.00012	0.08593
H2-15-57	317	35	0.00055	0.06544	0.00050	0.08545
H2-15-49	354	40	0.00096	0.06434	0.00090	0.08504
H2-15-42	394	40	0.00133	0.06458	0.00134	0.08467
H2-15-33	433	30	0.00182	0.06514	0.00188	0.08418
H2-15-24	490	35	0.00247	0.06306	0.00245	0.08353
H2-15-16	535	35	0.00346	0.06216	0.00230	0.08254

Table C.6. The Raw Data for BCl₃-H₂-He Experiments (Tot. Vol. Flowrate: 207.25ml/min, y_{BCl₃0}=0.066, y_{H₂0}=0.115 and y_{He}=0.819)

Run Number	T _r (C)	t (min)	y _{HClf}	y _{BCl₃f}	y _{BHCl₂f}	y _{H₂f}
H2-20-65	262	35	0.00015	0.06355	0.00021	0.11485
H2-20-57	317	35	0.00075	0.06539	0.00070	0.11425
H2-20-49	354	40	0.00125	0.06464	0.00118	0.11375
H2-20-42	394	40	0.00175	0.06366	0.00175	0.11325
H2-20-33	433	30	0.00230	0.06481	0.00236	0.11270
H2-20-24	490	35	0.00310	0.06411	0.00311	0.11190
H2-20-16	535	35	0.00428	0.06032	0.00312	0.11072

Table C.7. The Raw Data for BCl₃-H₂-He Experiments (Tot. Vol. Flowrate: 207.31ml/min, y_{BCl₃0}=0.066, y_{H₂0}=0.143 and y_{He}=0.791)

Run Number	T _r (C)	t (min)	y _{HClf}	y _{BCl₃f}	y _{BHCl₂f}	y _{H₂f}
H2-25-65	262	35	0.00023	0.06517	0.00031	0.14277
H2-25-57	317	35	0.00097	0.06547	0.00089	0.14203
H2-25-49	354	40	0.00154	0.06436	0.00144	0.14146
H2-25-42	394	40	0.00208	0.06396	0.00207	0.14092
H2-25-33	433	30	0.00261	0.06412	0.00273	0.14039
H2-25-24	490	35	0.00359	0.06179	0.00358	0.13941
H2-25-16	535	35	0.00498	0.06188	0.00382	0.13802

Table C.8. The Raw Data for BCl₃-H₂-He Experiments (Tot. Vol. Flowrate: 207.38 ml/min, y_{BCl₃0}=0.066, y_{H₂0}=0.172 and y_{He}=0.762)

Run Number	T _r (C)	t (min)	y _{HClf}	y _{BCl₃f}	y _{BHCl₂f}	y _{H₂f}
H2-30-65	262	35	0.00033	0.06545	0.00042	0.17167
H2-30-57	317	35	0.00115	0.06425	0.00107	0.17085
H2-30-49	354	40	0.00182	0.06371	0.00171	0.17018
H2-30-42	394	40	0.00239	0.06340	0.00239	0.16961
H2-30-33	433	30	0.00298	0.06150	0.00308	0.16902
H2-30-24	490	35	0.00408	0.06000	0.00409	0.16792
H2-30-16	535	35	0.00555	0.06339	0.00438	0.16645

Table C.9. The Raw Data for BCl₃-H₂-He Experiments (Tot. Vol. Flowrate: 207.44 ml/min, y_{BCl₃0}=0.066, y_{H₂0}=0.200 and y_{He}=0.734)

Run Number	T _r (C)	t (min)	y _{HClf}	y _{BCl₃f}	y _{BHCl₂f}	y _{H₂f}
H2-35-65	262	35	0.00043	0.06367	0.00050	0.19956
H2-35-57	317	35	0.00131	0.06478	0.00123	0.19868
H2-35-49	354	40	0.00202	0.06387	0.00191	0.19796
H2-35-42	394	40	0.00259	0.06280	0.00264	0.19738
H2-35-33	433	30	0.00333	0.06159	0.00345	0.19664
H2-35-24	490	35	0.00459	0.06027	0.00454	0.19537
H2-35-16	535	35	0.00616	0.06336	0.00492	0.19379

Table C.10. The Raw Data for BCl₃-H₂-He Experiments (Tot. Vol. Flowrate: 207.5 ml/min, y_{BCl₃o}=0.066, y_{H₂o}=0.228 and y_{He}=0.706)

Run Number	T _r (C)	t (min)	y _{HClf}	y _{BCl₃f}	y _{BHCl₂f}	y _{H₂f}
H2-40-65	262	35	0.00053	0.06542	0.00061	0.22747
H2-40-57	317	35	0.00152	0.06392	0.00142	0.22648
H2-40-49	354	40	0.00221	0.06469	0.00211	0.22579
H2-40-42	394	40	0.00293	0.06309	0.00297	0.22507
H2-40-33	433	30	0.00369	0.06310	0.00384	0.22431
H2-40-24	490	35	0.00505	0.06198	0.00499	0.22295
H2-40-16	535	35	0.00661	0.06095	0.00528	0.22139

Table C.11. The Raw Data of Reproducibility (Tot. Vol. Flowrate: 218.2 ml/min, y_{BCl₃o}=0.065 and y_{H₂o}=0.938)

Run Number	T _r (C)	t (min)	y _{HClf}	y _{BCl₃f}	y _{BHCl₂f}	y _{H₂f}
ReproBCl3-4-65	266	35	0,00149	0,06529	0,00134	0,93251
ReproBCl3-4-57	315	35	0,00304	0,06540	0,00287	0,93096
ReproBCl3-4-49	352	30	0,00464	0,06484	0,00494	0,92936
ReproBCl3-4-42	393	40	0,00676	0,06369	0,00743	0,92724
ReproBCl3-4-33	435	40	0,00892	0,06064	0,00943	0,92508
ReproBCl3-4-24	490	35	0,01190	0,05069	0,01071	0,92210
ReproBCl3-4-16	535	35	0,01557	0,06044	0,01109	0,91843

APPENDIX D

THE RESIDENCE TIME DISTRIBUTION OF REACTOR

The residence time distribution is determined experimentally by injecting an inert chemical, molecule or atom, called a tracer, into the reactor at time $t=0$ and then measuring the tracer concentration, C_{tracer} , in the effluent stream as a function of time. In addition to being a nonreactive species that is easily detectable, the tracer should have physical properties similar to those of the reacting mixture, and be completely soluble in the mixture (Fogler, 1992). Residence time distribution experiment is necessary to determine the behavior of the reactor used in the experiments. For this reason, a set-up was prepared for the performance of RTD (Figure D.1). Methane was used as a tracer. Helium was used as a carrier gas. The FT-IR was used to detect the methane concentration in the effluent gas mixture. Because FT-IR gas cell has a volume, a period of time is essential to reach the steady state. Two experiments were performed. First experiment was performed to determine the steady state time of gas cell and second was the RTD experiment of CSTR. The area of the CH_4 concentration in the first experiment was subtracted from the area of CH_4 concentration obtained in the second experiment.

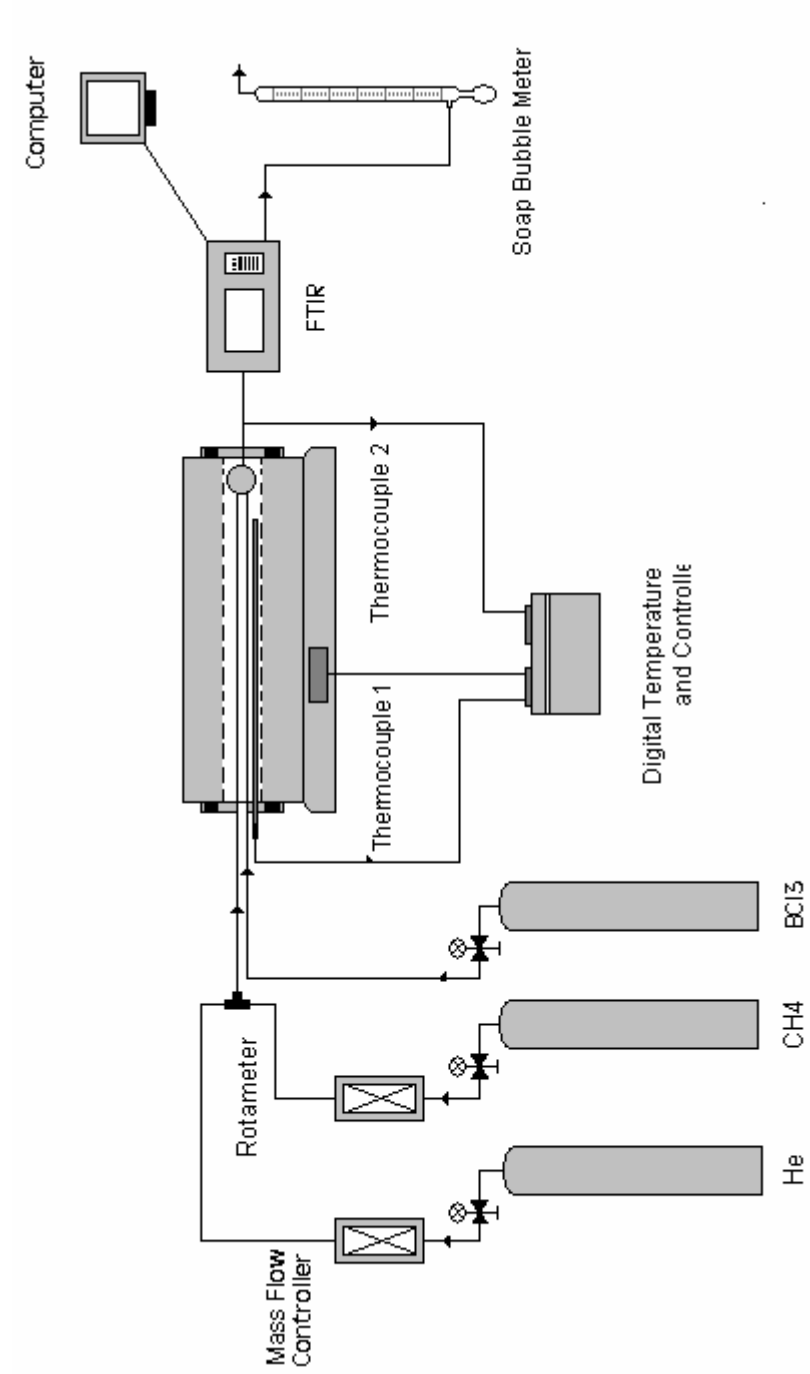


Figure D.1.1. Experimental Set-up for Characterization of Reactor

In the RTD experiments, experimental conditions were the same with the previous experiments. The gas cell temperature was 110°C and the total volumetric flow rate of the gas mixture was $200 \times 10^{-6} \text{ m}^3/\text{min}$. A pulse effect in the concentration of methane was done and concentration change of CH_4 with time was recorded.

In a pulse input, an amount of tracer N_0 is suddenly injected in one shot into the feed stream entering the reactor in short time. The outlet concentration is then measured as a function of time (Fogler, 1992). In the experiment, the pulse input was given using a rotameter. The methane tube was connected to the rotameter to measure the amount of CH_4 given as impulse. In both experiments (with reactor and FT-IR and with FT-IR only), an impulse of the same magnitude and duration was given. The volumetric flow rate of He was adjusted by using mass flow controller. The data for the RTD experiments are given in Table D.1-D.2.

Table D.1 Residence Time Distribution Experiment for Determination of the Steady State Time of Gas Cell

Run No	Time (min)	H_{CH_4}	Run No	Time (min)	H_{CH_4}
RTD-GC-0	0	0,000	RTD-GC-14	14	0,813
RTD-GC-1	1	0,022	RTD-GC-15	15	0,802
RTD-GC-2	2	0,090	RTD-GC-16	16	0,793
RTD-GC-3	3	0,188	RTD-GC-17	17	0,770
RTD-GC-4	4	0,248	RTD-GC-18	18	0,739
RTD-GC-5	5	0,331	RTD-GC-19	19	0,702
RTD-GC-6	6	0,403	RTD-GC-20	20	0,639
RTD-GC-7	7	0,485	RTD-GC-21	21	0,590
RTD-GC-8	8	0,588	RTD-GC-22	22	0,533
RTD-GC-9	9	0,635	RTD-GC-23	23	0,489
RTD-GC-10	10	0,710	RTD-GC-24	24	0,400
RTD-GC-11	11	0,748	RTD-GC-25	25	0,352
RTD-GC-12	12	0,765	RTD-GC-26	26	0,323
RTD-GC-13	13	0,789	RTD-GC-27	27	0,280

Table D.2 The Raw Data for the Residence Time Distribution Experiment.

Run No	Time (min)	H _{CH4}	Run No	Time (min)	H _{CH4}
RTD-0	0	0,000	RTD-21	42	0,384
RTD-1	2	0,239	RTD-22	44	0,359
RTD-2	4	0,429	RTD-23	46	0,335
RTD-3	6	0,525	RTD-24	48	0,307
RTD-4	8	0,629	RTD-25	50	0,286
RTD-5	10	0,697	RTD-26	52	0,267
RTD-6	12	0,744	RTD-27	54	0,248
RTD-7	14	0,766	RTD-28	56	0,230
RTD-8	16	0,781	RTD-29	58	0,213
RTD-9	18	0,767	RTD-30	60	0,197
RTD-10	20	0,748	RTD-31	62	0,180
RTD-11	22	0,720	RTD-32	64	0,167
RTD-12	24	0,696	RTD-33	66	0,154
RTD-13	26	0,659	RTD-34	68	0,141
RTD-14	28	0,624	RTD-35	70	0,131
RTD-15	30	0,599	RTD-36	72	0,120
RTD-16	32	0,553	RTD-37	74	0,113
RTD-17	34	0,513	RTD-38	76	0,106
RTD-18	36	0,485	RTD-39	78	0,102
RTD-19	38	0,450	RTD-40	80	0,097
RTD-20	40	0,413	RTD-41	82	0,093

The Figure D.2, D.3 and Figure D.4 were drawn by considering the Table D.1 and Table D.3. Figure D.2 is the RTD of gas cell and Figure D.3 contains the RTD of reactor and gas cell. For this reason, to determine the RTD of reactor only, these two figures (Figure D.2 and Figure D.3) were subtracted from each other. Finally, the Figure D.4 was obtained. It is seen that the response time of the reactor is very close to the residence time (0.58 min).

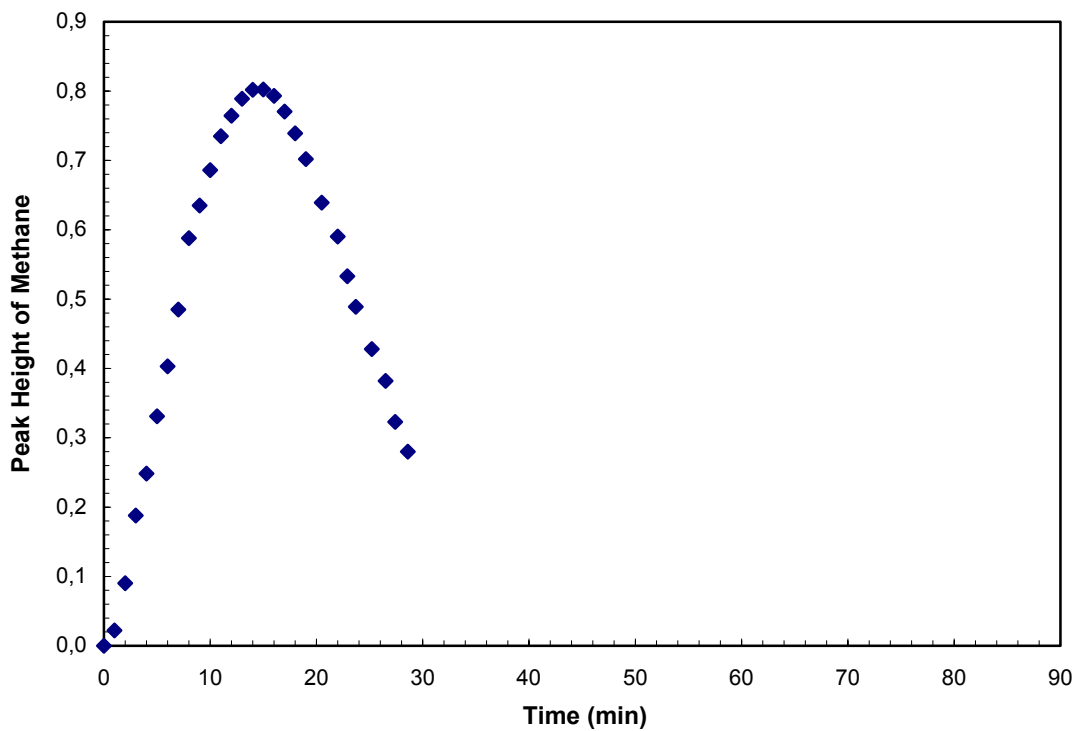


Figure D.2 Change of Methane Peak Height with Time for the Gas Cell

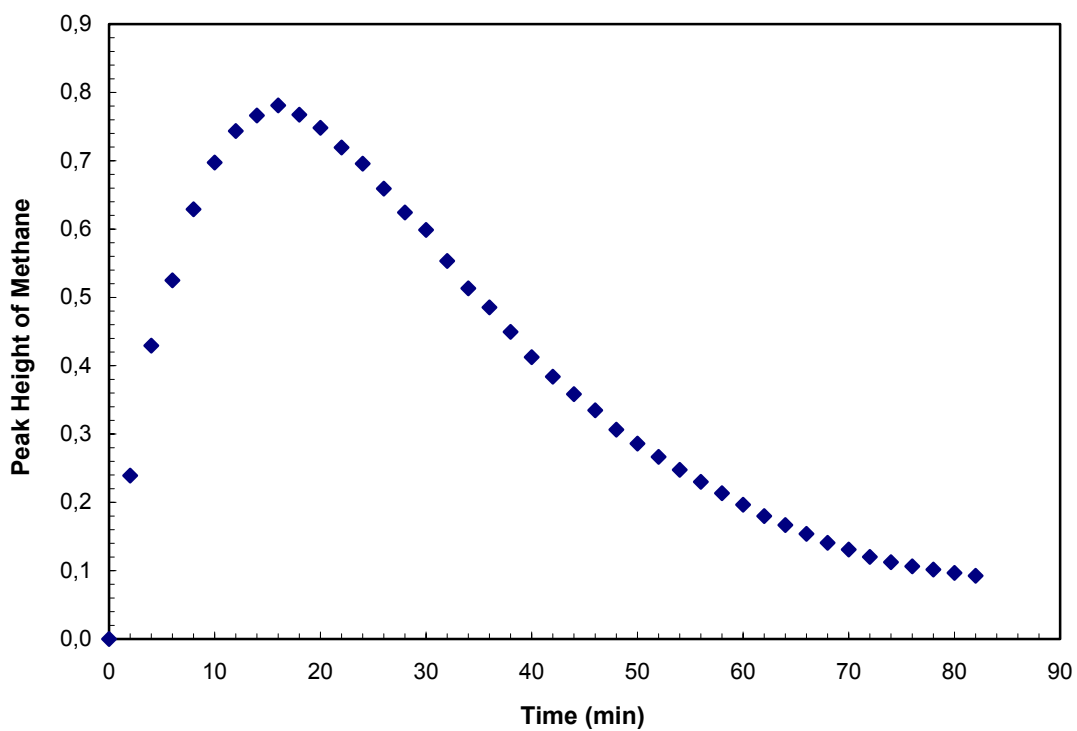
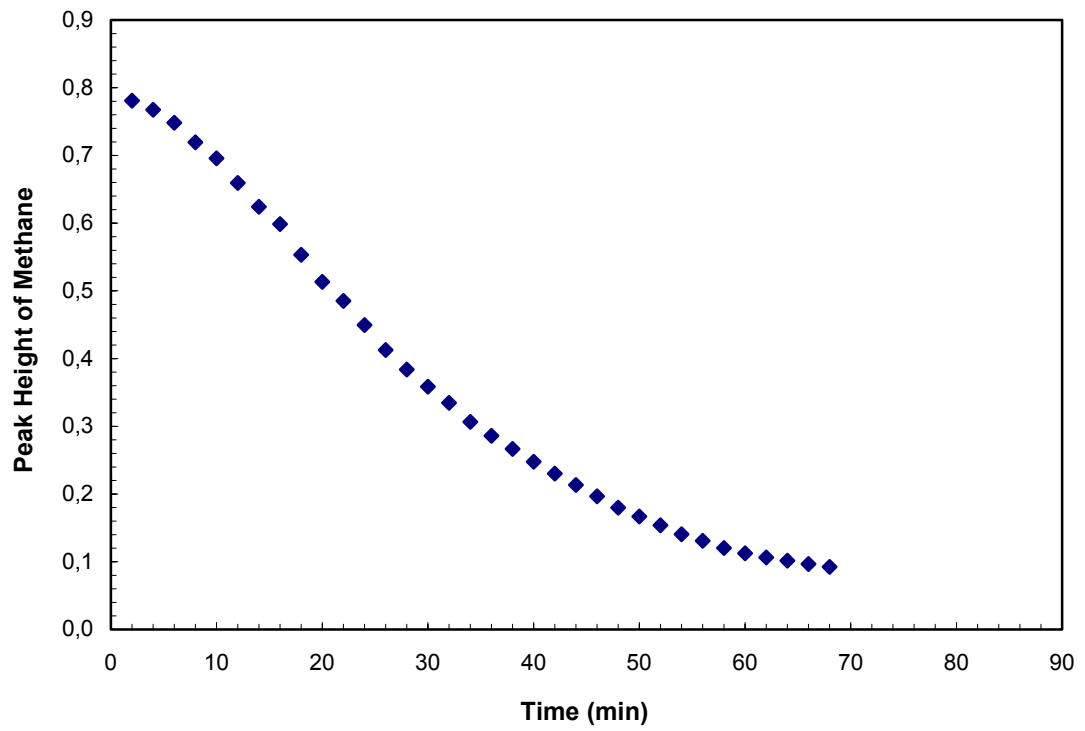


Figure D.3 Change of Methane Peak Height with Time for Reactor and Gas Cell



**Figure D.4 Change of Methane Peak Height with Time for Reactor Only,
Obtained by Taking the Difference of Curves Given in Figure D.2
and Figure D.3**